Slurry Based Three Dimensional Printing (S-3DP^{TM}) of Tungsten Carbide Cobalt

by
Mark A. Oliveira

B.S. Chemical Engineering
Worcester Polytechnic Institute of Technology. 2000

Submitted to the Department of Materials Science and Engineering in Partial Fulfillment of the Requirements for the Degree of

Master of Science in Materials Science and Engineering

At the
Massachusetts Institute of Technology

June 2002

Signature redacted

Signature of Author:_____
Department of Materials Science and Engineering
June 7, 2002

Signature redacted

Certified by: _____
Professor Michael J. Cima
Sumitomo Electric Industries Professor of Materials Science and Engineering
Thesis Supervisor

Signature redacted

Accepted by:_____
Professor Harry L. Tuller
Professor of Ceramics and Electronic Materials
Chairman, Departmental Committee on Graduate Students

Slurry Based Three Dimensional Printing (S-3DP™) of Tungsten Carbide Cobalt

by

Mark A. Oliveira

Submitted to the Department of Materials Science and Engineering
On April 1, 2002 in Partial Fulfillment of the
Requirements for the Degree of Master of Science in
Materials Science and Engineering

ABSTRACT

Multiple material systems were examined for the development of a Slurry Based Three Dimensional Printing (S-3DP™) process for micron scale tungsten carbide-cobalt (WC-Co) powders. The non-aqueous slurry was formulated with Polyvinylpyrrolidone (PVP) 10,000 dispersant, Poly(ethylene glycol) (PEG) 400 redispersant, and Isopropyl Alcohol (IPA). It was possible to successfully create cutting tool insert geometries with the S-3DP system using Vector Drop on Demand (DoD) printing and an aqueous Polyethylenimine 10,000 binder. Zephrym PD7000 and Solsperse 20,000 were also tested as dispersants for the non-aqueous slurry but were not suitable. Powder beds formed with these dispersants failed to redisperse after heating or aging in air. Experimentation focused on measuring the stability of all the slurries through rheology, jetting reliability, sedimentation density, slip cast density, sintered density, and sintered microstructure. Multiple binder materials such as Poly(acrylic acid), Polyethylenimine, cyanoacrylate glues, and Poly(vinyl acetate) were studied for their compatibility with the slurry systems and ability to form strong green parts. Slurry transport techniques were developed to overcome drying and settling sensitivity issues. Raw material properties such as particle size, density, specific surface area, and oxygen content for the WC and Co powders were measured. IR absorption, elemental microanalysis, molecular weight determination, and curing temperature were measured for the dispersant, redispersant, and binder materials.

Thesis Supervisor: Prof. Michael J. Cima

Title: Sumitomo Electric Industries Professor of Materials Science and Engineering

TABLE OF CONTENTS

LIST OF FIGURES

LIST OF TABLES

ACKNOWLEDGEMENTS

First of all I would like to thank my advisor, Professor Michael Cima. Throughout the many twists and turns, and sometimes dead ends, of the project his leadership has taught me how to learn from each situation and then to proceed to the main goal.

Thanks to Professor Emmanuel Sachs for his support and guidance through every step of the project. He showed me how to keep things in perspective, and I learned to temper my scientific curiosity into why something may not work with knowing when to move on in order to get results.

I would also like to express my thanks to Kennemetal and Valenite for their technical and financial support throughout this project. In particular I would like to thank Dr. Russ Yeckley and Dr. John Keane for all their help, as well as Dave Siddle and John Freiderichs.

Thanks to all my friends in the 3DP group and in the CPRL. I constantly relied on every one of them for help and always got the help I needed, even in their busiest of times.

Most of all, thanks to my family and my loved ones who have always been there for me, and without which I would not be where I am today. Thanks to Marissa who had more faith in me than I did and who kept me sane (for the most part) through college and grad school. Finally, special thanks to my Mom who has always kept her sons as her number one priority through the hardest times and taught me about strength and determination.

1 Introduction

1.1 Three-Dimensional Printing (3DP^{TM})

3DP is a Solid Freeform Fabrication (SFF) technique developed at MIT. The process generates three-dimensional shapes by combining sequential two-dimensional layers. The 3-dimensional shapes are created without the use of a mold or machining with a short amount of time between the design and production stages, as with other SFF techniques. Another advantage of the process is its flexibility to accommodate a number of material systems. Thus far, 3DP has been successfully applied to ceramic, metal, polymer, and composite systems.

There are two approaches to 3DP, traditional 3DP and slurry based 3DP (S-3DP). The two processes differ by the manner in which the layers are created. Dry powder is spread from a reservoir with a vibrating roller over a piston to create the layers in traditional 3DP. A 2-dimensional image of the component cross section is generated from a CAD file and a binder material is then ink-jet printed into selected areas of the spread powder to define this 2-D shape. The binder penetrates into the pores of the powder layer and adheres the particles within that layer and to the layer below. The piston is lowered, another layer of powder is spread, and the process is repeated until a 3-dimensional shape has been created. The powder in areas where binder is printed serves as a support during the printing process and then is removed once printing is completed. Figure 1 illustrates this process.

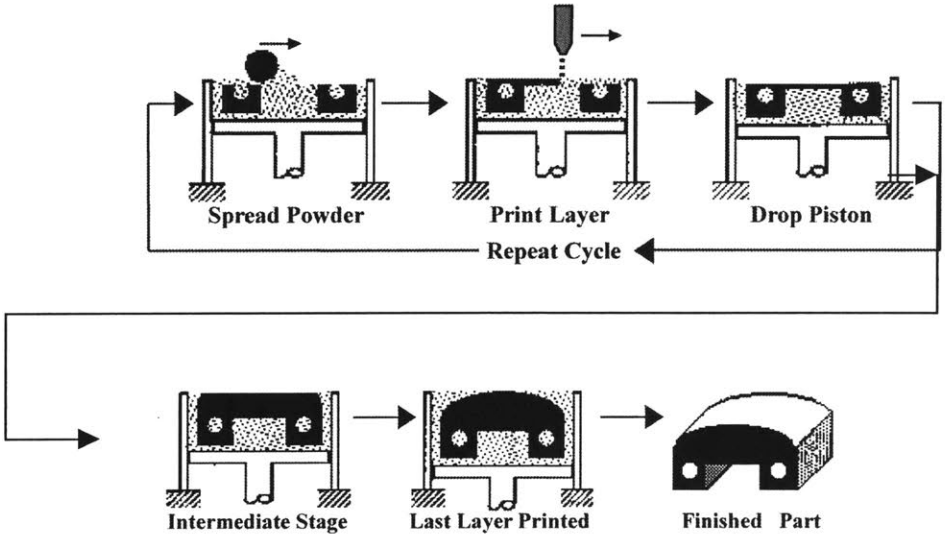

Figure 1: Schematic of the traditional (dry-powder) 3DPTM process.

1.2 Slurry Based Three-Dimensional Printing™ (S-3DP™)

Slurry Based Three-Dimensional Printing was developed at MIT for the rapid production of electronic and structural ceramic components. These applications require ceramic powders in the micron to sub-micron size range. Powders of this scale are not suitable for dry powder spreading since van der Waals forces cause these powders to stick together. The attraction between the particles hinders them from flowing freely and causes dry spread beds to pack non-uniformly and develop cracks. This effect, combined with the high incidence of agglomerates, decreases the packing density of dry spread beds to a level below that needed for sintering to full density.

Slurry processing techniques were introduced in order to handle the powder. A slurry, or slip, is made by dispersing the powder in a liquid medium. Ionic stabilization, steric stabilization, or a combination of both is used to achieve this in either an aqueous or non-aqueous system. The slurry is jetted through a small diameter nozzle that is then raster scanned across a porous substrate, enabling the individually jetted lines to form a

single slip cast powder layer. The bed is then dried using a heat lamp or hot air to remove the excess liquid and the binder material is ink jet printed into the layer. As in the traditional 3DP process, the layers are formed on a piston that is lowered after each cycle.

Another difference between S-2DP and traditional 3DP is the method used to retrieve printed parts. The excess powder in S-3DP powder beds has significant strength and cannot be removed by brushing or using compressed air. Instead, slip cast powder beds are submersed in a liquid and sonicated to retrieve the printed parts. The S-3DP process is outlined in Figure 2.

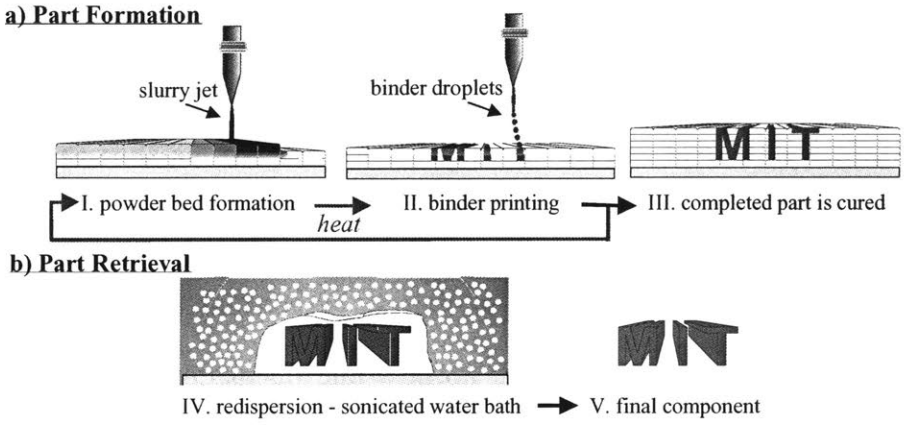

Figure 2: Schematic of the Slurry-Based 3DP™ (S-3DP™) Process.

1.3 Motivation

The ultimate goal for the work with the WC-Co system at MIT and of this thesis is to produce WC-Co cutting tool inserts using the S-3DP process and a non-aqueous slurry system. The slurry system consisted of either Solsperse 20,000 (Avecia Inc.) or Polyvinylpyrrolidone (Sigma-Aldrich) 10,000 as the steric dispersant in an isopropyl alcohol medium. These systems were in initial development at the end of a previous

project. The work in this thesis continues the investigation into these systems as a possible means to produce WC-Co cutting tool inserts. The requirement for a non-aqueous system is due to the reactivity of the cobalt in water. Observation of WC and Co powders showed that the Co dissolved in water and reprecipitated as an oxide or oxy-hydroxide. It is undesirable for the Cobalt to oxidize in an aqueous slurry. Zanetti[1], et al. showed that the combination of WC and Co particles in an oxygenated aqueous environment caused the break down organic molecules through the generation of free radicals at the interface of the Co and WC particles. Gothelid[2], et al., showed that during the sintering of WC-Co the presence of oxygen as CoO clusters on the WC surface prevented the Co from wetting the surface of the WC, and thus halted the sintering process.

The primary areas of interest for the development of the slurries, parts and , powder beds made from them, are:

1. Jetting Reliability— The slurry must be able to be jetted through a small diameter orifice for multiple hours with little or no flow rate fluctuations to produce powder beds.
2. Binder Compatibility — The binder system must be able to infiltrate into the bed to attach the powder particles together with sufficient strength..
3. Redispersion Ability— Printed 3DP parts must be retrievable from the powder bed through placement in a liquid medium to remove the excess powder with little requirement for sonication.

4. Sintering — The powder bed and printed 3DP parts must be capable of being sintered to greater than 99% of theoretical density with an acceptable pore rating and a proper stoichiometry and microstructure.

Success in these four areas is needed in order to have an acceptable S-3DP process. The first and last requirements deal with slurry stability and processing techniques which control such things as green density, void formation, and agglomerate formation. Low green density and void formation during printing result in poor sintering results. Agglomerate formation, through poor slurry stability or drying during processing, results in poor jetting reliability. Requirements 2 and 3 were controlled by the nature of how components in the materials system react with one another. Binder compatibility with the surface of the powder and existing adsorbed polymers affected surface adhesion, which affected part strength. Chemical reactions between the dispersant and the binder also affected part strength and binder infiltration. All of these factors will be explored in the remainder of the thesis.

2 Previous Work with S-3DP™ and WC-Co

This chapter provides background information related to the new work reported in this thesis. The first section of this chapter is an introduction to the controlling parameters for the S-3DP™ process. Next, the governing principles behind powder bed redispersion and binder infiltration are discussed. Finally, previous work accomplished with WC-Co at MIT is reported.

2.1 S-3DP™ Process Parameters

This section will discuss the process parameters used to control the layer height of the slip cast layers and the binder content in a printed part.

2.1.1 Slurry Deposition

A model was created to predict the layer height, LH, of individual ceramic layers. Figure 3 illustrates the model used for layer height calculation. Layers are formed by rastering a slurry jet across a porous substrate. The individual slurry lines merge together to form a single layer, as was discussed in the previous chapter. The layer height is calculated by performing a mass balance on a volumetric element of deposited slurry. The slurry flow rate, Q_S, is divided by the print speed, v, and the slurry line spacing, LS_S, to get the thickness of a layer of un-cast slurry, LH_S.

$$LH_S = Q_S / (v \bullet LS_S) \tag{2.1}$$

The flow rate of the slurry is measured directly while the print speed and slurry line spacing are set in the controller software. With the appropriate conversion factors the slurry layer height, LH_S, in micrometers is the result. Since this is the height of a wet slurry line it must be multiplied by the fraction of solid powder in the slurry, f_S, and

divided by the packing fraction of the slip cast powder bed, PF, to get the cast layer height, LH.

$$LH = (LH_S \bullet f_S) / PF \tag{2.2}$$

The packing fraction is measured through experimentation and the fraction of solid powder is set during slurry formulation.

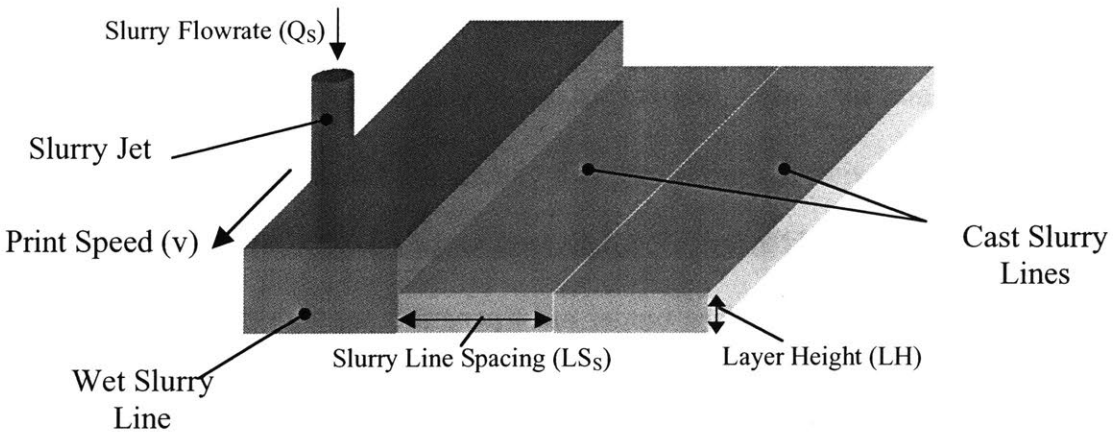

Figure 3: Model used for Layer Height calculation (not to scale).

2.1.2 Binder Deposition

The strength of the printed part depends on the amount of binder that can be printed into the powder bed for a given binder material. This amount is expressed as the volume percent of the binder with respect to the powder. There is a lower limit to this volume percent that must be exceeded for the parts to be strong enough to survive redispersion and handling. There must also be enough binder so that it can penetrate through one ceramic layer to the layer below. This ensures that the 2-dimensional cross sections printed into the part knit together and form a single 3-dimensional part after printing. The upper limit to the binder content is set by the amount of pore space in the powder bed. There is also a practical upper limit to the binder content where it must be low enough during printing so that there is enough pore space for subsequent layers to

slip cast properly. Another limiting factor is the need to reduce the amount of organic material that must be removed before sintering. The binder content in the powder bed must be low enough so that it can be removed completely, or to a sufficient extent, during a burnout step before sintering. Any binder that is not removed in this step is left behind in the sintered part as residual carbon, which may adversely affects material properties. Residual carbon left in WC-Co powder beds precipitates as graphite. These graphite precipitates are very week and act as pores that reduce the strength of the sintered material.

The amount of binder to be delivered to the powder bed is dependant upon the ceramic layer height, *LH*. The binder must penetrate through the ceramic layer to the next below in order to stitch the layers together as illustrated in Figure 4.

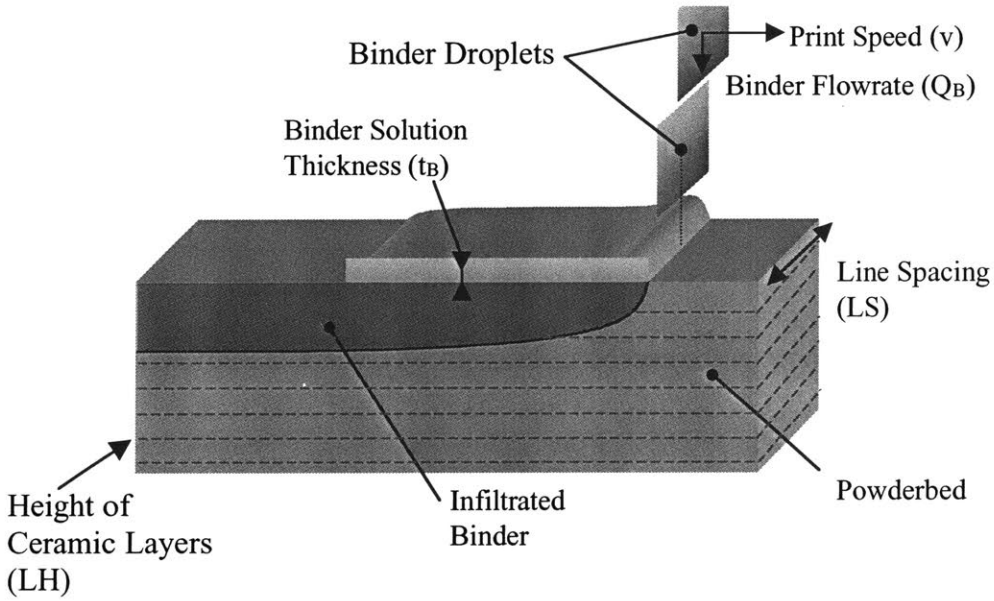

Figure 4 Model used for Binder saturation ratio calculation (not to scale). The dashed lines indicate the height of individual slurry layers in the bed.

The volume of liquid deposited in a given length is divided by the volume of pore space in the ceramic layer for that same given length to calculate the binder penetration depth. The thickness of an imaginary layer of binder, t_B, is calculated by dividing the

volumetric flow rate of the binder solution, Q_B, by the print speed, v, and line spacing, LS to accomplish this.

$$t_B = Q_B / (v \bullet LS) \tag{2.3}$$

Next, the thickness of the pore volume per unit length, t_P, is calculated by multiplying the thickness of a cast layer of powder bed, LH, by the fraction of pores in a powder bed, (1-PF).

$$t_P = LH \bullet (1\text{-}PF) \tag{2.4}$$

Assuming that the binder solution completely fills the pore space as it infiltrates into the powder bed, and that the binder does not adsorb to the surface of the powder particles, the saturation ratio is calculated by:

$$SR = t_B / t_P \tag{2.5}$$

It can be seen upon inspection that the saturation ratio gives the depth the binder will be deposited into the bed in multiples of the layer thickness. This ratio must be kept above 1 in order to ensure that the individual ceramic layers will knit together to form a 3-dimensional shape.

The volumetric ratio of solid binder to powder is calculated by dividing the thickness of the solid binder layer per unit length, t_{SB}, by the thickness of the solid powder layer per unit length, t_{SP}.

$$Vol\ \% = (t_{SB} / t_{SP}) \text{ x } 100 \tag{2.6}$$

where:

$$t_{SB} = t_B \bullet f_B \tag{2.7}$$

and

$$t_{SP} = LH \bullet PF \tag{2.8}$$

with f_B being the fraction of solid binder in the binder solution.

Holman showed that if the solid binder in the binder solution adsorbs to the surface of the powder particles, then the depth to which the binder penetrates is not the same as that of the advancing binder solution. Experiments directly measuring the depth of penetration of the solid binder are needed in order to determine the proper printing parameters in this case. Holman also showed that the shape that an individual droplet of binder takes in the powder bed, known as the binder primitive, is a result of multiple competitive processes. These are the spreading of the liquid on the surface of the bed in competition with its infiltration into the powder bed as well as the adsorption of solid binder onto the surface of the powder[3]. This phenomenon is discussed in more detail in a later section.

2.1.2.1 Differential Slip Casting

Differential slip casting is a process anomaly encountered with S-3DP when printing binder into powder beds and is illustrated in Figure 5. The casting rate of slurry over a printed region is lower than over an unprinted region. This occurs when slurry is deposited on a powder bed layer that has an interface between a printed and unprinted region. The height of the slurry layer decreases faster in the areas with a greater slip casting rate causing the slurry to migrate laterally to these regions from the areas with a slower slip casting rate. The result is a depression of the bed height over the binder-printed areas combined with a slight height increase in the unprinted region immediately adjacent to this area. Figure 6 shows the effect differential slip casting has on a WC-Co bed.

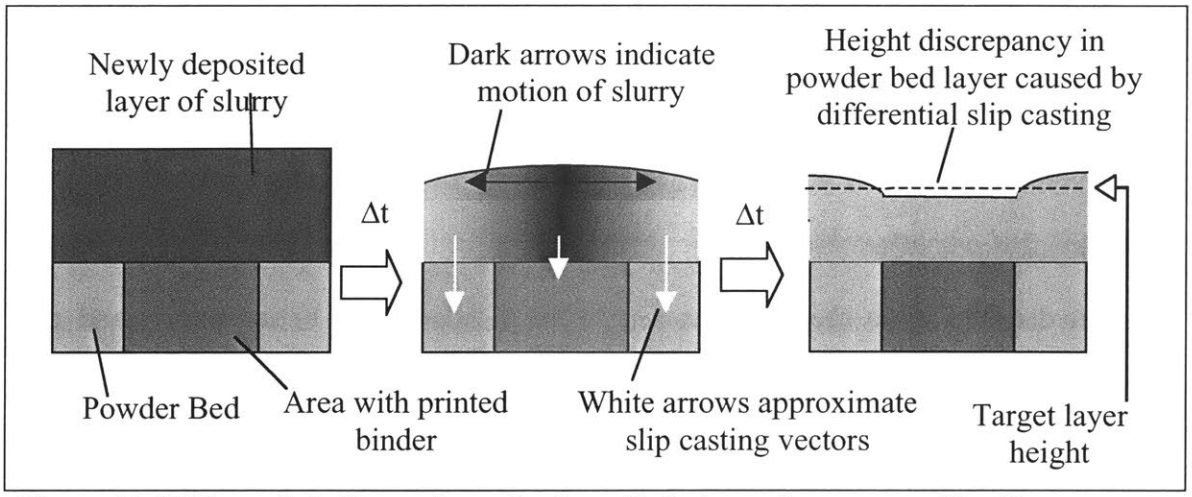

Figure 5: Differential slip casting of a deposited slurry layer caused by the presence of binder in the powder bed.

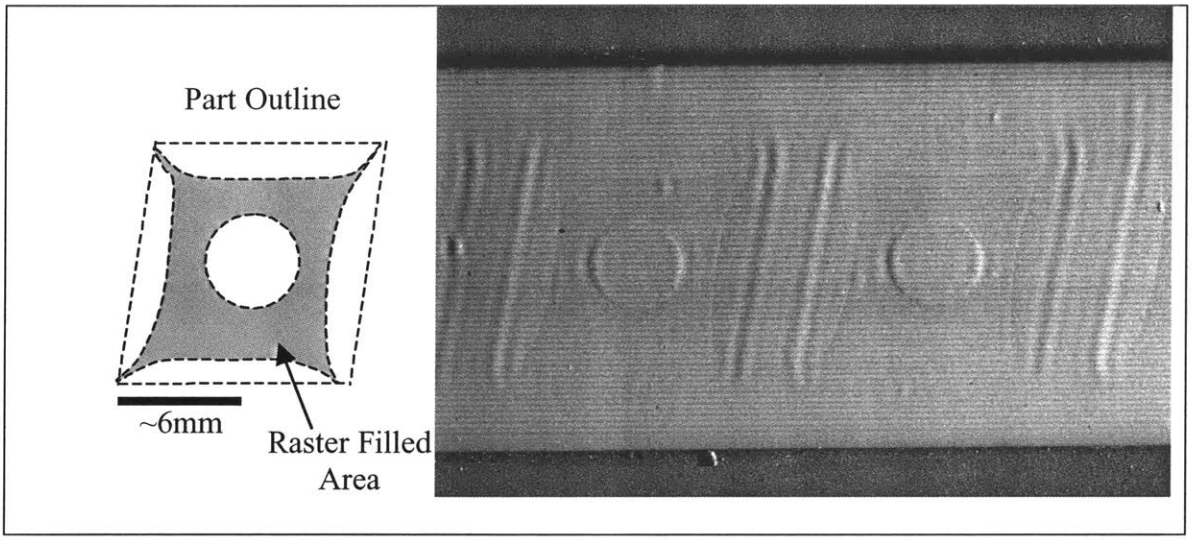

Figure 6: Top view of a WC-Co bed with printed cutting tool inserts. Low angle lighting shows the effects of differential slip casting.

2.2 Redispersion of Powder Beds

Printed parts are retrieved from a powder bed by placing the bed in a liquid medium, called the redispersion solvent. Originally, sonication was needed to break up the powder in the unprinted regions in order to remove it. This mechanical means of part retrieval has been replaced by chemically swelling the bed. Upon immersion of a powder

bed into the redispersion solvent, the liquid is observed to infiltrate into the bed. Initially, this occurs slowly with no dimensional changes and is driven by capillary forces. Once the pore space in the powder bed has been filled the bed begins to swell. Uhland[4] has proposed that osmotic pressure is the driving force for the continued flux of liquid into the powder bed once the pore space has been filled. To better understand this phenomenon it is useful to restate this as the osmotic pressure developed by the solution within the pores pushes the powder bed apart. The powder bed areas that are not held together by binder lose strength when this happens. The swelled powder bed begins to fall away from the part on its own, and can easily be washed away without the need for sonication. This process is of particular importance for parts designed with through or blind holes or for parts with delicate fine-scaled features that may be damaged by extensive sonication. Figure 7 shows the swelling process in an S-3DP printed powder bed.

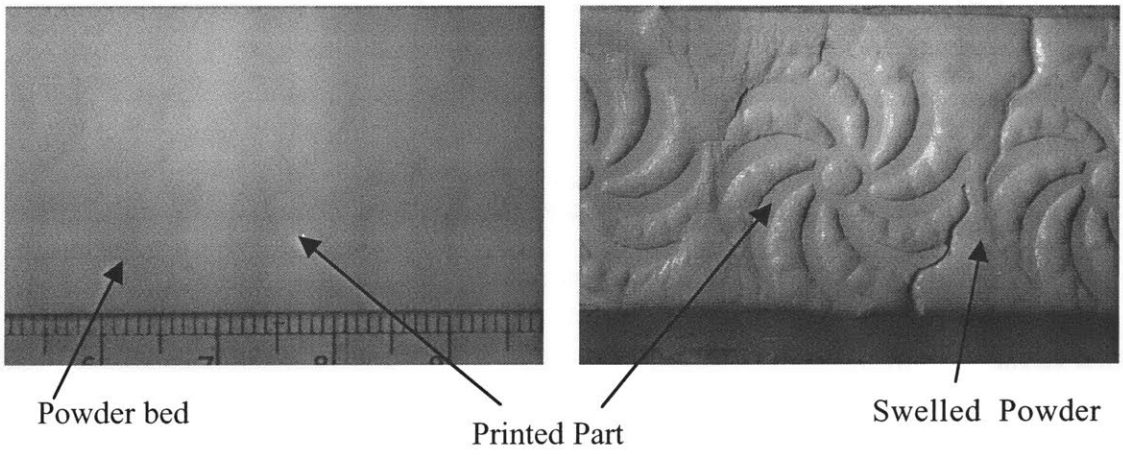

Figure 7: Images of swelling of MR2 powder bed during redispersion[5]

A redispersing agent needs to be added to the powder bed to achieve the osmotic pressure necessary to redisperse the bed. This redispersant is added to the slurry before the powder bed is made. During slip casting the slurry solvent evaporates, leaving the

redispersant behind. This redispersing agent resides in the pores of the bed and dissolves when the bed is placed into the redispersion solvent. The choice of the redispersant-solvent system is important since the osmotic pressure is a property of this system. Knowledge is required about of the strength of the powder beds being formed and of the magnitude of osmotic pressures that can be developed to make this choice,. Uhland measured the strength of alumina, silica and titania powder beds to be in the range of 0.1 to 0.6 MPa. Using aqueous Poly(ethylene glycol) (PEG) solutions, which can produce osmotic pressure far exceeding 0.6 MPa[5], he determined the minimum PEG concentrations needed to overcome the strength of the powder beds.

2.2.1 Osmotic Pressure of Solutions

Discussions on osmotic pressure can be found in textbooks that deal with solution thermodynamics. This section will give a brief overview of the subject as it applies to S-3DP™ in terms of polymer solutions.

A common experiment that reveals the effect of osmotic pressure is performed by separating a pure solvent and a polymer solution with a semipermeable membrane, which allows only the solvent molecules to pass through it. The solvent will flow into the solution to try and equalize its chemical potential on both sides of the membrane. The flow of solvent into the solution will ultimately be stopped by the increase in pressure caused by the volumetric expansion of the solution. This pressure is the osmotic pressure. Figure 8 illustrates this process.

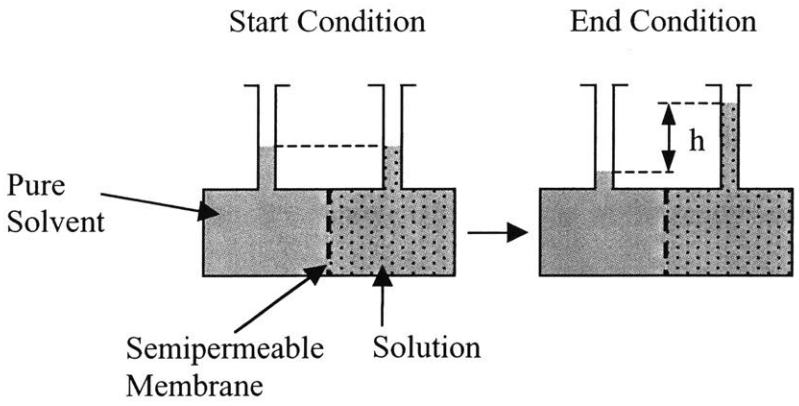

Figure 8 Osmotic Pressure experiment. In this setup the osmotic pressure can be measured from the height difference of the liquid columns.

The thermodynamic reasons for this can be explained by the following argument. The free energy of a system at constant temperature and pressure can be written as,

$$dG = \Sigma \mu_i dn_I \tag{2.9}$$

where G is the free energy, μ_i is the chemical potential of component *i*, and n_i is the number of moles of component *i*. If there are multiple phases in the system, and we designate each phase as *A*, *B*, etc. then,

$$dG = dG_A + dG_B + \ldots \tag{2.10}$$

Equilibrium requires that $dG = 0$, therefore we can combine (2.9) and (2.10) for the two phase system shown in Figure 8 to get

$$\mu_{i,A}\, dn_{i,A} = \mu_{I,B}\, dn_{i,B} \tag{2.11}$$

with conservation of matter between the two phases this equation becomes

$$\mu_{i,A} = \mu_{I,B} \tag{2.12}$$

The equation shows that the chemical potential of the pure solvent must equal the chemical potential of the solvent in the solution. The chemical potential of component *i* in a solution at constant temperature and pressure can be written as,

$$\mu_i = \mu_i^o + RT(ln\ a_i) \tag{2.13}$$

where R is the gas constant, T is the temperature in Kelvin, μ_i^o is the chemical potential of pure component i, and a_i is the activity of component i in the solution. We can replace the subscript i with *1* to indicate the solvent and *2* to indicate the solute. The chemical potential has its greatest value for a pure substance, with the activity of the component equal to 1. Addition of a second component decreases the activity to less than 1 and also decreases the chemical potential from that of a pure substance by an amount $RT(ln\ a_i)$ since the natural log of a number less than 1 is negative. Also, from thermodynamics it is known that any increase in the pressure of the system will increase the chemical potential of the component. It can be seen that the osmotic pressure is generated to counteract the decrease in chemical potential caused by the addition of a second component in order to keep the chemical potential on the solution side of the membrane equal to that on the pure solvent side. This relationship can be written with the following equation.

$$\mu_1^o = \mu_1^o + RT(ln\ a_1) + \int V_1 dp \tag{2.14}$$

where V_1 is the partial molar volume of the solvent and the integral is evaluated from the initial pressure to the initial pressure plus the osmotic pressure, π. Assuming that V_1 is constant and rearranging to solve for osmotic pressure, equation (2.14) becomes,

$$\pi = -RT(ln\ a_1) / V_1 \tag{2.15}$$

Combining equations (2.13) and (2.15) gives the relationship between chemical potential and osmotic pressure,

$$\mu_1 = \mu_1^o - \pi V_1 \tag{2.16}$$

Equation (2.15) shows that for a pure solvent in which a_1 is zero there is no osmotic pressure. But as the activity becomes less than 1 from the addition of a second component, and $ln\ a_1$ becomes increasingly negative, the osmotic pressure increases.

The activity in equation (2.15) can be replaced by the mole fraction x_1 for an ideal solution. Expanding the logarithm, and keeping only the leading order terms, equation (2.15) becomes,

$$x_2 = \pi V_1 / (RT) \tag{2.17}$$

If the solution is dilute,

$$x_2 = n_2/(n_1 + n_2) \approx n_2 / n_1 \tag{2.18}$$

where n_i is the number of moles of component i. Substituting into (2.17) produces the van t Hoff equation,

$$n_2 = (n_1 \pi V_1) / (RT) \ = \pi V_1^{\ T} / (RT) \tag{2.19}$$

where $V_1^{\ T}$ is the volume of the solvent in the solution, $n_1 V_1$.

The process of expanding the logarithm to produce equation (2.17) must include a correction factor for each mole fraction term in the power series to include the effects of nonideality. Ignoring higher order term and rearranging to convert mole fraction units to concentration units produces,

$$\pi / (RTc) = 1/M_2 + Bc \tag{2.20}$$

where M_2 is the molecular weight of the solute, c is the solute concentration, and B is the second virial coefficient. Equation (2.20) obeys the van t Hoff equation at infinite dilution. One important result of this equation is that a plot of $\pi/(RTc)$ versus concentration provides the molecular weight of the solute from the intercept. Also, it can

be seen that as the molecular weight of a polymer increases, the osmotic pressure developed decreases.

Equation (2.20) has been further expanded by the Flory-Huggins theory. Considering the entropy of mixing through statistical thermodynamics and the enthalpy of mixing through the interaction energy of the solvent and solute molecules, the change in chemical potential was written as,

$$\mu_1 - \mu_1^o = RT(ln\ \phi_1) + RT(1\text{-}1/n)\ \phi_2 + \chi\phi_2^2 \qquad (2.21)$$

where ϕ_i is the volume fraction of component i, n is the number of polymer segments, and χ is the Flory-Huggins interaction parameter, or chi parameter. χ is a measure of the pairwise interaction of the solvent and solute molecules. Combining this equation with equation (2.16), and rearranging to be in the form of equation (2.20) gives the Flory-Huggins equation[6],

$$\pi/(RTc) = 1/M_2 + [(1/2\text{-}\chi)/V_1](V_2/M_2)^2 c \qquad (2.22)$$

Equations (2.15) and (2.22) are very important to the S-3DP process because they can be used in conjunction with tabulated chi-parameter values and the values of activity for many polymer solutions that can be found in the literature[7,8,9,10,11]. These tabulated values can be used to help find a new or better redispersant-solvent system if needed.

2.3 Binder Infiltration

The previous section outlined the controlling parameters of binder deposition and in it the importance of adsorption, spreading, and infiltration was briefly introduced. This section will discuss these phenomenon in more detail.

Holman[3] showed that polymer adsorption onto the surface of the powder particles affected the depth of binder penetration into the powder bed. He concluded that the solid

binder contained within the binder solution filtrates from the solution by adsorbing to the surface of the particles as the liquid penetrates into the powder bed. The binder solution concentration decreases until a point is reached where all the solid binder has been removed from the solution and the advancing liquid is just the solvent.

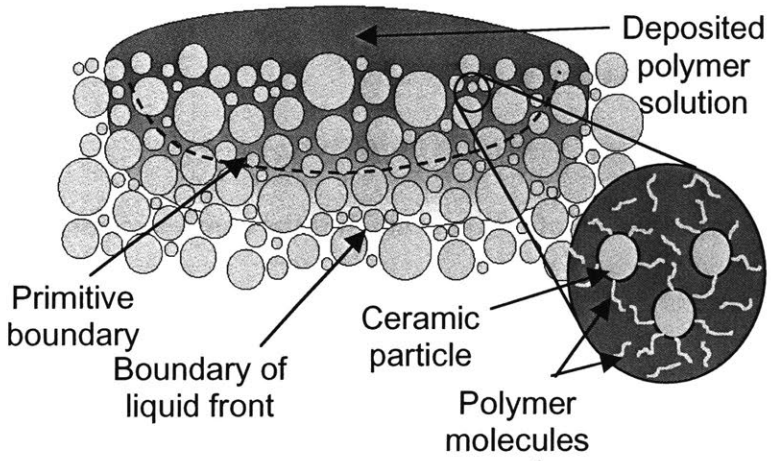

Figure 9: Illustration of binder filtration mechanism[3].

Holman used an aqueous binder solution of Polyacrylic Acid (PAA) with alumina, titania, and silica powder beds of approximately the same size and specific surface area. The PAA dissociates in aqueous solutions and becomes negatively charged. The surfaces of the alumina, titania, and silica powders at the pH of PAA solutions carry a positive, neutral, and negative charge, respectively. Adsorption isotherms performed with the powder showed that PAA adsorbed the strongest to the surface of alumina with less adsorption on the titania and no appreciable adsorption was seen with the silica. Tests were performed in S-3DP powder beds by forming single lines of binder with equivalent doses of binder solution. These lines were then retrieved and cross-sectioned. The results coincided with the adsorption isotherms, which showed that cross sectional area increased from the alumina, to silica beds. These results determined that the surface charge of a powder affects the adsorption of the PAA binder and the depth that the solid

binder can penetrate into the powder bed. Holman also showed that particle size also affected infiltration depth through the use of 3 different alumina particle sizes of 0.3, 0.6, and 1.7 μm. The decreasing particle size increased the specific surface area of the powder from 1.2 m^2/g to 8.6m^2/g. The results showed that the cross section of binder primitive lines decreased with the increasing specific surface area of the powder, as is expected in an adsorption filtration process.

Another aspect of his work focused on the factors controlling the width of the binder primitive lines. He concluded that two main processes controlled this width, 1) the rate at which the binder spreads over the surface of the powder bed due to its equilibrium contact angle and 2) the infiltration rate of the binder into the powder bed. As the binder spreads over the surface of the powder bed after impact, its advance is halted then reversed by its infiltration into the powder bed. Previously it was believed that the time scale of these two processes was very different and that only one of these was a controlling parameter. Testing showed, however, that this was not always the case and that their relative rates depended on particle size. This can be seen in Figure 10, which shows the diameter of binder droplets versus time after impact on top of alumina powder beds of two different particle sizes[12].

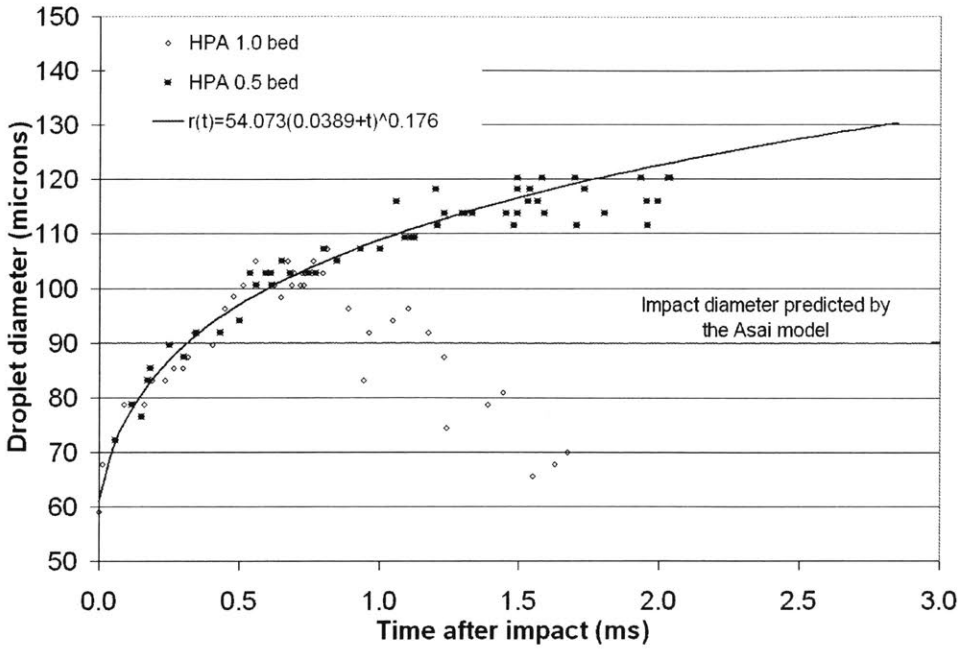

Figure 10: Diameter of liquid droplet on top of an alumina powder bed as a function of time. Data collected for two different particle sizes of 0.3 (HPA 0.5) and 0.6μm (HPA 1.0)[3]

The data shows that while the spreading of the droplet across the surface of the bed occurs at the same rate for the two different particle sizes, the point at which infiltration starts to decrease the diameter of the drop occurs much sooner in the powder bed with the larger particle size. Using different particle sizes in the beds controls when spreading is overcome by infiltration and this controls the width of binder lines that are created. The results of the model for predicting this behavior is shown in Figure 11. The increasing curve predicts the diameter of a binder droplet as it spreads from a minimum diameter on top of a powder bed. The decreasing curves predict the diameter of a binder droplet from an initial maximum diameter as it infiltrates into a powder bed for varying particle sizes. The point at which the curves intersect is the predicted width of the binder primitive. The dependence on particle size can be understood by realizing that pore size

varies proportionally with particle size, and it is the pore size that is one of the controlling factors for infiltration rate.

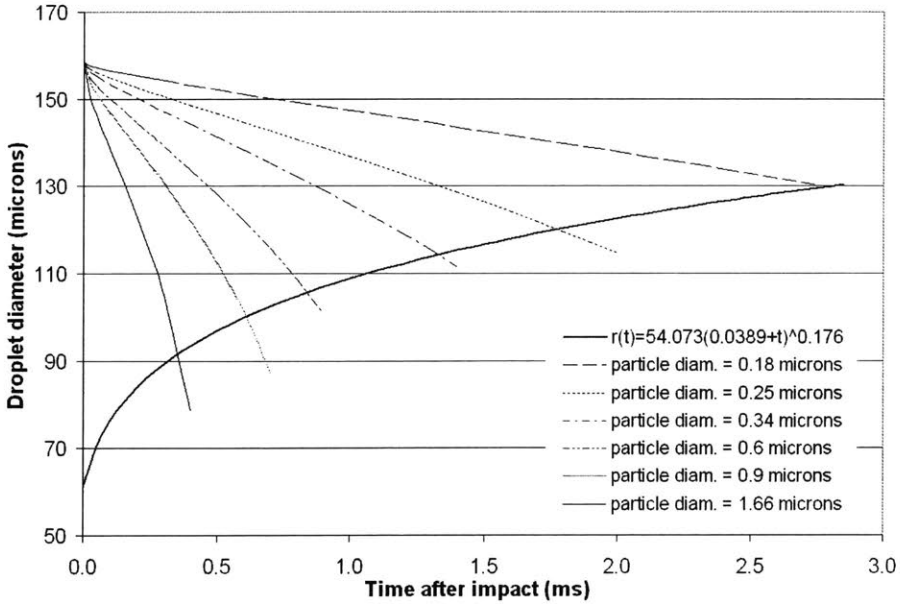

Figure 11: Predicting ultimate binder line width by varying particle size[3].

2.4 Previous Work with WC-Co

Guo[13] experimented with WC-Co systems in order to find suitable slurry compositions with which to perform S-3DP. Initial work focused on many different solvent-dispersant systems with only WC powders. The performance of these systems was evaluated by measuring the sedimentation densities of slurries with 10 and 13 volume percent solids. The systems with the best performance were then tested with WC-Co powders, of which one was chosen to proceed with powder bed formation experiments. The dispersants that were tested with WC-Co powders, and the solvent they were used with, are shown in Table 1.

Dispersant	Solvent
OLOA (Chevron Corp.)	Heptane
Emphos PS-21A (Witco Corp.)	Isopropyl Alcohol
Menhaden Fish Oil (Omega Protein, Inc.)	Isopropyl Alcohol
DePhos HP-739 (DeForest Enterprises, Inc.)	Isopropyl Alcohol

Table : 1 Previously investigated WC-Co slurry systems[13]

The OLOA-Heptane system showed the highest sedimentation densities (43%) for the 10vol% slurries tested. The system was not chosen for further experimentation because the Heptane is toxic and it attacks or swells most plastics which complicated the printing process. The Emphos-IPA system was chosen for further investigation because it gave the next best performance (33% sedimentation density) while meeting the criteria for non-toxicity.

The Emphos slurry had 25vol% solids loading and was milled for approximately 80 hours. Rheology measurements determined that the slurry was shear thinning, leveling off to a viscosity of 90 cP at a shear rate of 400 s^{-1}. The slurry also exhibited a yield stress of about 12 Pa. The Emphos slurry was used to create jetted S-3DP beds. These beds attained green densities of 50-54% theoretical with a bimodal pore size distribution of 0.12 and 0.22 μm. Sintered densities of about 98% were achieved. The sintered microstructures of the beds showed pores in the 5 - 7 μm size range. The reason for these pores was not determined. Laser profilometry of optimized powder beds showed a surface peak to valley roughness of 10 μm. Initial tests on redispersion were conducted by using slip cast discs of the WC-Co slurry. These small discs were slip cast by placing a volume of slurry that contained the PEG within a permeable mold and

allowing the solvent to be drawn out with time. The results of these tests suggested that the PEG did not help the slip casts to redisperse. The WC-Co slip casts were also tested with an aqueous PAA binder to determine their compatibility. A 2.4vol% PAA-water binder with 10wt% (of PAA) Glycerol was used. The tests consisted of measuring the strength of green WC-Co bend bars and comparing the results with similar green bend bars that had been infiltrated with the PAA binder and cured. The results did not indicate that the binder was increasing the strength of the bars, and it was concluded that the binder was not compatible with the system. Guo suggested that the binder solution was not infiltrating into the powder beds since it was observed to take 2-3 hours to disappear from the surface of the beds. Instead of infiltrating into the part, the solvent was simply evaporating and the PAA was left at the surface of the part. Guo concluded that while the Emphos-IPA system produced good results, a new slurry system was needed in order to provide a stable slurry and better results.

Two dispersants used in Isopropyl alcohol were tested to achieve this. The first was Polyvinylpyrrolidone (PVP)-MW 10,000, whose chemical structure is shown in Figure 12a. The PVP slurry had a 30vol% solids loading and 0.5dw% (weight% of the dry powder). The viscosity of the slurry was 30cP, which was much lower than the 90cP measured for the Emphos slurry. Jetting of the powder beds was achieved with far fewer nozzle clogs, as well. This suggested that the PVP slurry was more stable than the Emphos slurry. Powder beds made from the PVP slurry showed a lower green density, 45%, but sintered to greater than 99% theoretical density and did not show the 5 — 7 μm voids that were present in the Emphos powder beds. When the PVP powder beds were tested with the aqueous PAA binder, a reaction between the PAA and the PVP was

observed. A gelation reaction was taking place as the binder was being printed into the powder bed, which caused it to segregate to the surface, shown in Figure 12b. This caused problems with the slip casting of the subsequent layers and the printed parts exhibited delamination during the redispersion process[14].

a)

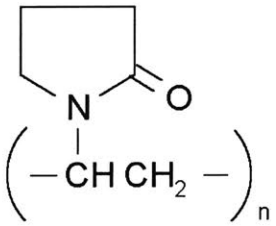

b)

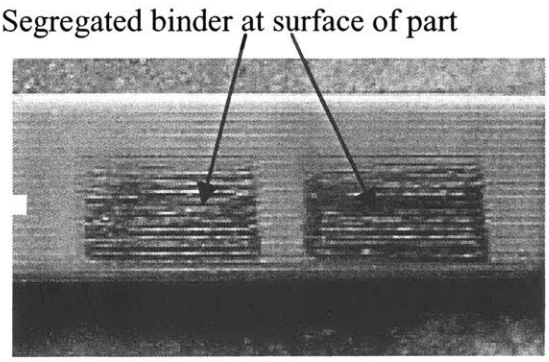

Figure 12 a) Chemical structure of Polyvinylpyrrolidone. b) PVP powder bed showing the segregation of PAA binder at the surface

The second dispersant to be tested was Zephrym PD 7000. This was a proprietary dispersant obtained from Uniquema Inc, so no chemical structure could be obtained. The green density of the powder beds were 46% of theoretical, and they were sintered to >99% of theoretical. The powder beds also did not show the 5 — 7 μm voids that were seen in the Emphos powder beds. The beds also featured a low surface roughness of 7.3 ±0.3 μm. Parts printed with the PAA binder were retrieved from the Zephrym powder beds. These parts required sonication for removal since the beds did not redisperse after the binder cure step, even with the addition of Poly(propylene glycol) (PPG) to the powder beds as a redispersant. The PPG did, however, cause redispersion of the powder beds before the curing step. Figure 13 shows these results.

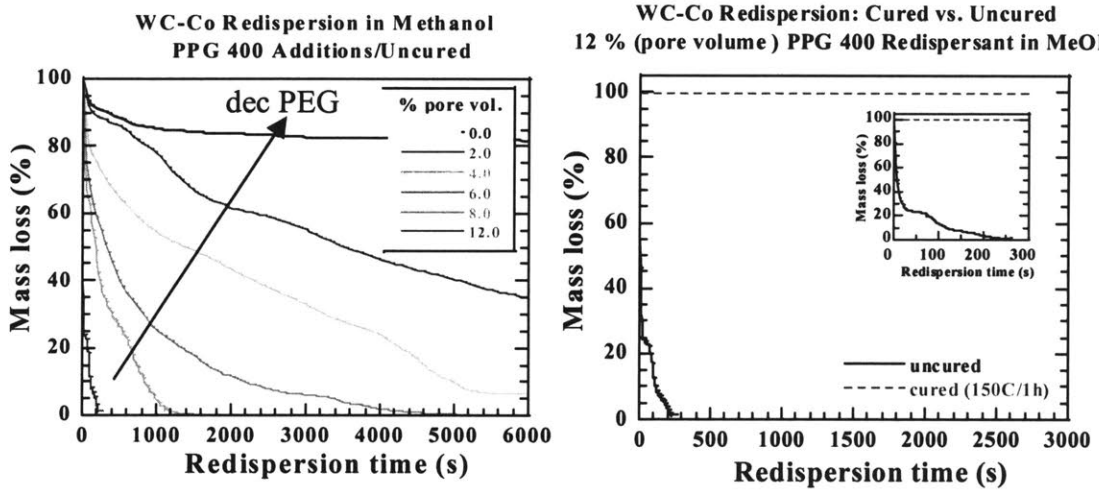

a b

Figure 13: a) Redispersion of WC-Co powder beds with varying PPG concentrations. b) Redispersion of WC-Co beds containing PPG before and after 150 °C/ 1hr binder cure step.

The packing fraction for the slurry was recorded as a function of dispersant concentration at two solids loadings. The data showed that the optimum dispersant concentration was at 0.5 wt% of the powder. At this point the packing fraction reached a plateau for both the 10vol% and 30vol% slurries.

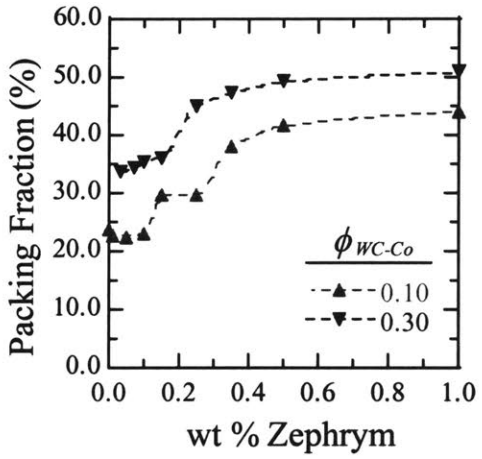

Figure 14: Packing fraction for 10vol% and 30vol% WC-Co slurries with Zephrym PD7000 dispersant

This work with Zephrym PD7000 marked the furthest experimentation conducted with the WC-Co system at the time that the work presented in this thesis was started. In comparison to the Emphos and PVP systems, the Zephrym system was seen as the best candidate material system for the S-3DP process at the time. The following chapters will describe the experiments performed with the Zephrym and PVP systems and discuss the result

3 Material System Formulation and Properties

This chapter will discuss the slurry system and the binder system used for S-3DP of Tungsten Carbide — Cobalt.

3.1 Slurry Systems

The WC-Co slurry used for S-3DP ranges from a 24 to a 28vol% solids loading. The solvent is a low water content Isopropyl Alcohol (IPA) (Omnisolve, VWR). Two dispersants were tested, Solsperse 20,000 (Avecia Inc.) and Polyvinylpyrrolidone MW=10,000 (Sigma-Aldrich). If necessary, Poly(ethylene glycol) 400 (PEG) was used as a redispersant and its concentration was varied from 0.5wt% to 1.6wt% of the powder. This section will discuss the raw materials used for the slurry and will be followed by the procedure for creating the slurry.

3.1.1 Powder Properties

The WC and Co powders are provided separately from Valenite Inc and Osram Sylvania, respectively. The WC powder is Valenite Inc. 1399 Carbide Grade Powder with a reported mean particle size of 0.8 μm and density of 15.3 g/cc. Measurements performed at MIT on a Horiba Capa-700 Particle Analyzer for the WC powder confirmed the 0.8 μm mean diameter and showed a particle size range from 0.1 to 1.4 μm. These results are shown in Figure 15. The density of the powder was measured to be 15.13 g/cc using a Quantachrome StereoPycnometer with Helium gas. The surface area of the powder was measured to be 1.114 m^2/g using a Quantachrome Quantasorb B.E.T with a 70 Helium: 30 Nitrogen gas mixture.

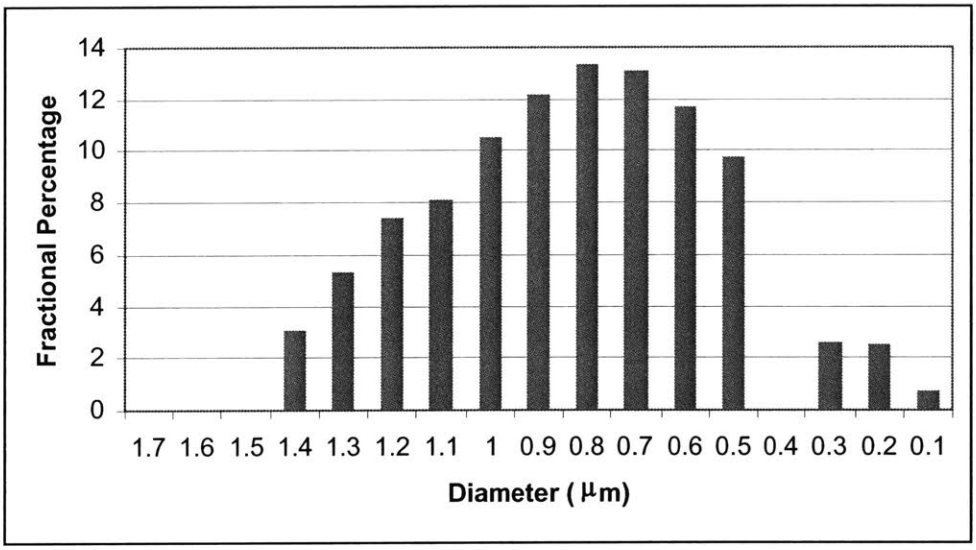

Figure 15: Particle size distribution for WC powder (as received).

The Co powder is Osram Sylvania extra fine cobalt powder with a reported mean particle size of 1.5 μm and ranged from 0.8 to 1.8 μm. The reported density of the powder is 8.6 g/cc. The density and surface area of the powder were measured to be 8.60 g/cc and 0.731 m^2/g with the same methods mentioned above with the WC powder. The particle size was verified through S.E.M. imaging of the as received powders, as shown in Figure 16.

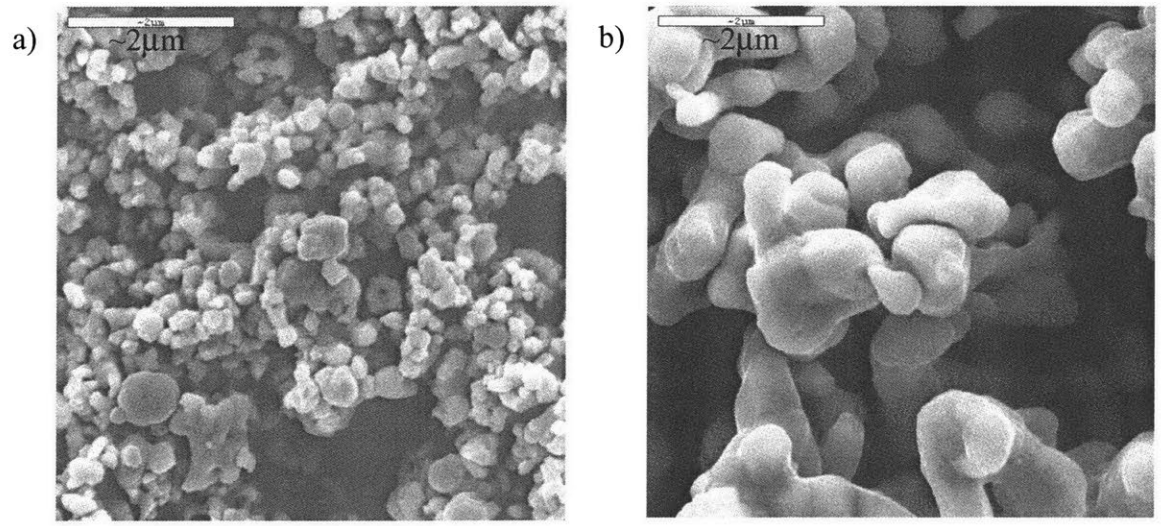

Figure 16 SEM image of as received a) WC and b) Co powders at equal magnification.

The surface of the WC powder is expected to oxidize to form WO_3 and carry a negative surface charge. Andersson, et al[15], reported that the surface of WC particles placed in water first oxidizes to WO_3 then dissolves, with the dissolution step considered to be rate limiting. The rate of dissolution changes very little over a pH range from 3 to 11, with dissolution rate constants of 1.3 $X10^{-7}$ to $1.9x10^{-7}$ mol m^{-2} hr^{-1}, respectively. The dissolution of WC in water is accompanied by a decrease in pH, thus the surface of the powder is acidic and carries a negative charge. The Co powder showed the opposite results, increasing pH as dissolution progressed because the surface of the powder is basic and carries a positive charge due to an oxide layer forming on the surface. The dissolution rate of the Co powder in aqueous WC-Co mixtures is highly dependant on pH. At pH values above 7 the dissolution rate constant is of the same order as the WC, but at low pH the Co powders dissolve much faster, with the rate constant reaching $260x10^{-7}$ mol m^{-2} hr^{-1} at a pH of 3. In aqueous mixtures of WC and Co the dissolution rate of the WC is decreased considerably at pH values below 10. Also included in the

work by Andersson were zeta potential measurements of WC in water. The effect of interaction with Co^{2+} ions was determined by using varying $CoCl_2$ concentrations. The zeta potential measurements of WC suspensions with no $CoCl_2$ were strongly negative in the 3-11pH range tested. The zeta potential became decreasingly negative with increasing $CoCl_2$ concentrations of 10^{-5},10^{-4}, and 10^{-3}M, and the isoelectric points were measured at a pH of 8.5, 8.2, and 8, respectively.

Testing of the WC and Co powder was performed at Kennemetal. 2 samples of WC and Co powder were mixed together and tested for oxygen content on a Leco oxygen analyzer. The test was a combustion process in which the sample of WC-Co was mixed with carbon. Oxygen combined with C to form CO and the CO was measured giving the total oxygen content of the powder. The first sample of powder was placed in water, and the second in isopropyl alcohol. Both samples were sonicated then centrifuged and the supernatant poured off. Methanol was then added to both samples and they were sonicated, centrifuged, and the supernatant removed to wash them. This was repeated once more before the samples were sealed and sent off for testing. The results are shown in Table 2.

Powder Sample	Oxygen Content-1st Sample	Oxygen Content-2nd Sample
WC-IPA	0.2701 wt%	0.273wt%
WC-Water	0.289wt%	0.336wt%

Table 2: Results of oxygen analysis of WC powder mixed with water and IPA.

The oxygen content of the IPA sample was considered to be normal for WC-Co powders. The increase seen in the water sample was considered to be within acceptable limits and not expected to pose any problems during sintering[16].

A third WC-Co powder was used in early experiments with this system, as well as the experiments reported in the previous chapter. The powder was a Valenite Inc. VC-101 grade powder. This is a premixed powder blend of the WC and Co powders described above with a Co content of 10wt%. The reported mean particle diameter is 0.8 μm, and the reported density of the powder is 14.46 g/cc. The mixing process contaminates the powder with a wax, which is added to aid in creating a homogeneous mix of the dry powders. The result of this contamination adversely affects slurry properties, which will be shown in the following sections discussing slurry rheology and the green density of powder beds.

3.1.1.1 Dispersant and Redispersant Properties

The dispersant, Solsperse 20,000 (Avecia Inc.), is a polymeric surfactant that is chemically equivalent to the Zephrym PD 7000 (Uniquema Inc.) dispersant which was used in the WC-Co slurry experiments reported Chapter 2. The change from Zephrym to Solsperse was necessary because Zephrym PD7000 was no longer being manufactured and a comparable dispersant was not made by Uniquema. Infrared absorption spectra, elemental analysis, and molecular weight measurements revealed that the dispersants were chemically the same. Figure 17 shows the infrared absorption spectra for both polymers that were performed on a Nicolet Impact 410 IR. The single point molecular weight determination tests as well as carbon, hydrogen, oxygen, and nitrogen elemental analysis were performed by Huffman Laboratories, Inc. Table 3 shows the results of these tests.

The results of the infrared absorption spectra show that the two dispersants match up at every peak, thus they both contain the same functional groups. The elemental

analysis shows that both dispersants contain the same ratio of atoms and the molecular weight determination shows that both dispersants have the same molecular weights. Taken together, these results determine that the two nonionic polymers are identical.

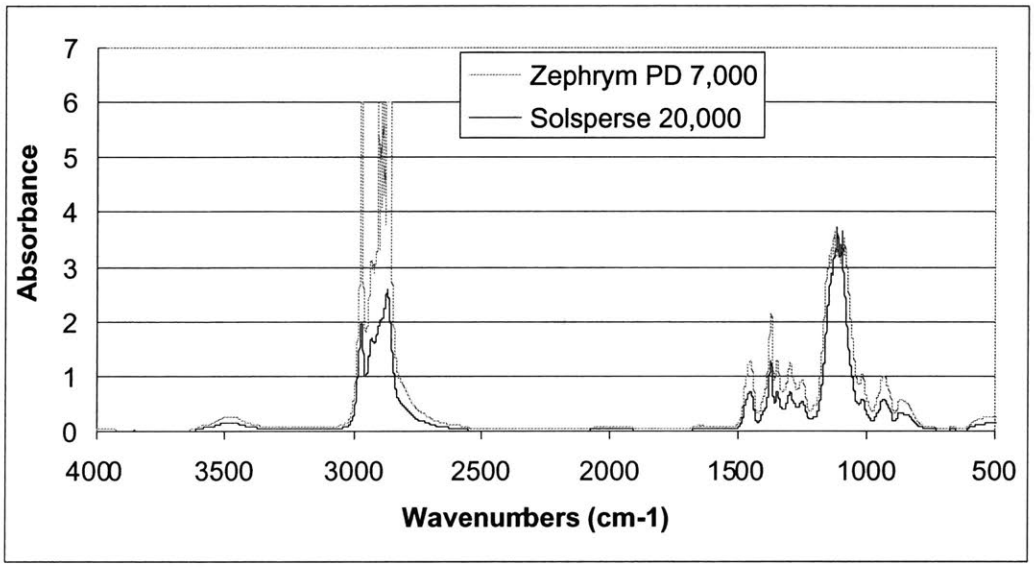

Figure 17 Infrared absorption scans of Solsperse 20,000 and Zephrym PD7000.

	Solsperse 20,000	Zephrym PD70000
Carbon Atomic%	60.09	59.90
Hydrogen Atomic %	10.11	10.10
Oxygen Atomic %	30.05	30.09
Nitrogen Atomic %	0.78	0.78
Molecular Weight (average of two samples)	1142	1155

Table 3 Results of elemental analysis and single point molecular weight determination for Solsperse 20,000 and Zephrym PD7000.

The Polyvinylpyrrolidone (PVP) dispersant was obtained from Sigma-Aldrich (cat# 85,645-2) with an average MW 10,000. The Poly(ethylene glycol) (Carbowax

PEG) added to the slurry as a redispersant has a molecular weight of 400. Its chemical structure is shown in Figure 18.

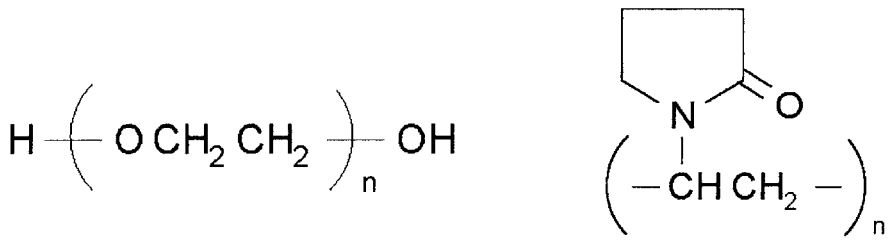

Figure 18 Chemical structure of Poly(ethylene glycol) (left) and Polyvinylpyrrolidone (right).

Tests were performed to determine the degree to which the Solsperse and PEG adsorb to the surface of the WC and Co powders. A sample of Co powder was placed in PEG-IPA or solution and sonicated. The suspension was then allowed to reach their equilibrium adsorption overnight. It was then centrifuged and the clear supernatant removed. Methanol was used to wash the powder twice, with samples of the powder taken after each wash. Finally, the powder sample was dried in a vacuum oven at 50°C to remove the methanol and then placed in a Perkin — Elmer TGA 7 Thermogravimetric Analyzer to measure the weight loss as they were heated to 450°C. The weight loss of the washed samples in the TGA was then compared to the weight loss of as received powder. The PEG remains on the surface of the powder after the methanol washes if it chemically bonds to the surface. This is seen as a difference in weight loss between the as received powder and the sample. A similar procedure was performed on WC-Co powder bed samples. The powder bed contained 0.5wt% Solsperse and 1.6wt% PEG. Samples of heat treated and non heat treated beds were washed in methanol. The heat treatment simulated the binder curing step and was a bake at 150°C for 1hr in an argon atmosphere. Both samples were shaken to break them apart before centrifuging and

washing. Samples were cured in order to determine if either the Solsperse or the PEG were crosslinking or decomposing during the step. A weight percent loss in the TGA that was less than the weight loss seen in the uncured bed is seen if the polymers were decomposing. An increase in weight loss from the uncured washed bed is seen if the polymers were crosslinking and forming an insoluble polymer that remained on the powder during the methanol washes. Results showed that the polymers were physically adsorbed weakly to the surface and no difference was seen between the as received Co powder and the washed Co powder. Also, there was no difference, within the detection capabilities of the machine, between the cured and uncured beds either before or after washing with methanol. These results are shown in Figure 19a and b.

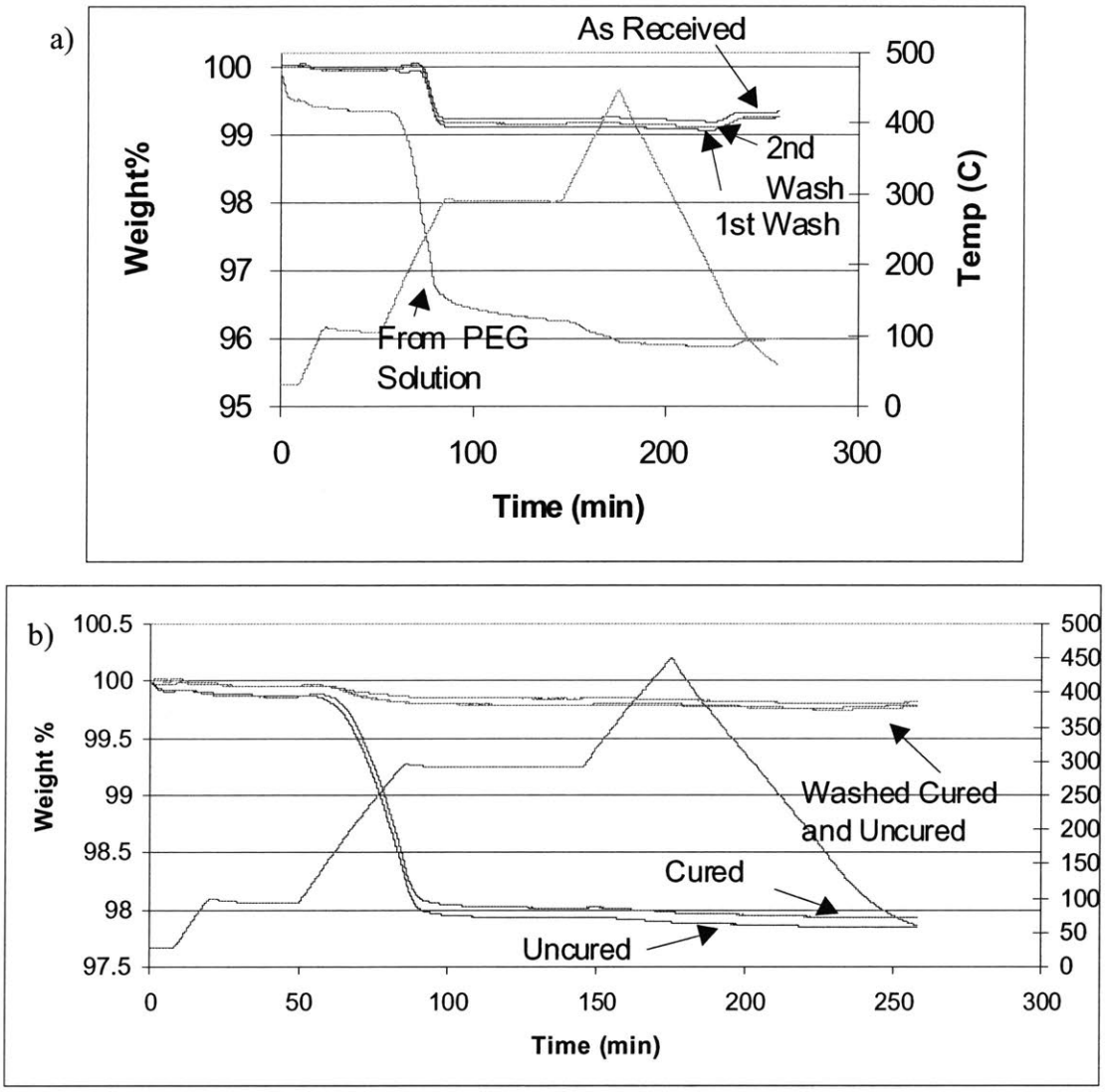

Figure 19 Thermogravimetric analysis of a)Co powder and b)WC-Co powder bed to determine extent of adsorption of Solsperse and PEG onto the powder surfaces.

3.1.2 Slurry Preparation

The dispersant was dissolved in IPA and then the WC milling media was added to prepare the slurry. Enough media was added to ensure good tumbling of the media during milling, and this normally meant filling 1/3 to _ of the container. Next the Co powder was added followed by the WC powder, which was added in 2 parts. The slurry was shaken between the addition of the powders in order to ensure good mixing before it

was placed on a ball mill. The slurry was then milled for 18 hours to break up agglomerates that formed while the powder was stored. If a redispersing agent was required, Poly(ethylene glycol) (PEG) was added to the slurry after milling.

3.1.3 Slurry Properties

Three primary slurry properties were tested to measure the stability of the slurry and determine the optimum slurry composition; the packing fraction of sedimented slurries, the viscosity of the slurry, and the green density of powder beds made with the slurry. The viscosity of the slurries was measured on a parallel plate Paar Physica DSR4000 Universal Dynamic Spectrometer. The green density of powder beds was measured by mercury intrusion porosimetry on a Micromeritics Autopore II 9220.

3.1.3.1 Packing Fraction

The packing fraction of the slurries was measured by placing a known volume of slurry into a graduated vial. The slurries were then allowed to settle out of suspension, forming a layer of packed powder that is clearly discernable form the liquid. The volume of the packed powder was recorded as well as the total volume of slurry that was placed in the vial. The actual volume of the powder was calculated by multiplying the total volume of the slurry by its solids loading, and then this number was divided by the volume of the packed powder to get the packing fraction. This value provides an estimate of the stability of the slurry. In a stable slurry the particles are well dispersed, settle slower, and pack to a higher density. In an unstable slurry the particles flocculate, settle faster, and pack to lower densities. This is illustrated in Figure 20.

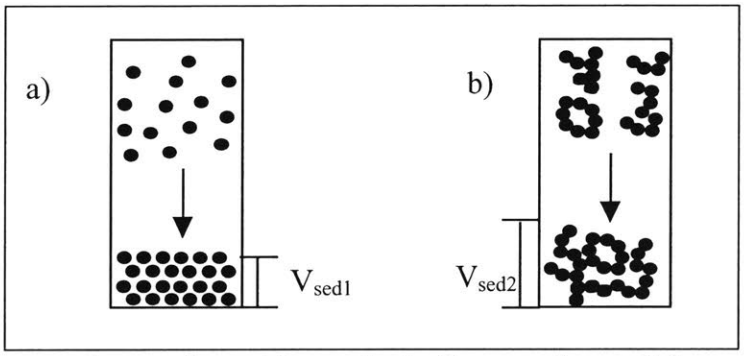

Figure 20 Comparison of packing of a) dispersed particles versus b) flocked particles.

Testing was performed to obtain the effect that varying the solids loading and Solsperse concentration has on the packing fraction. Figure 21 shows the results of these tests.

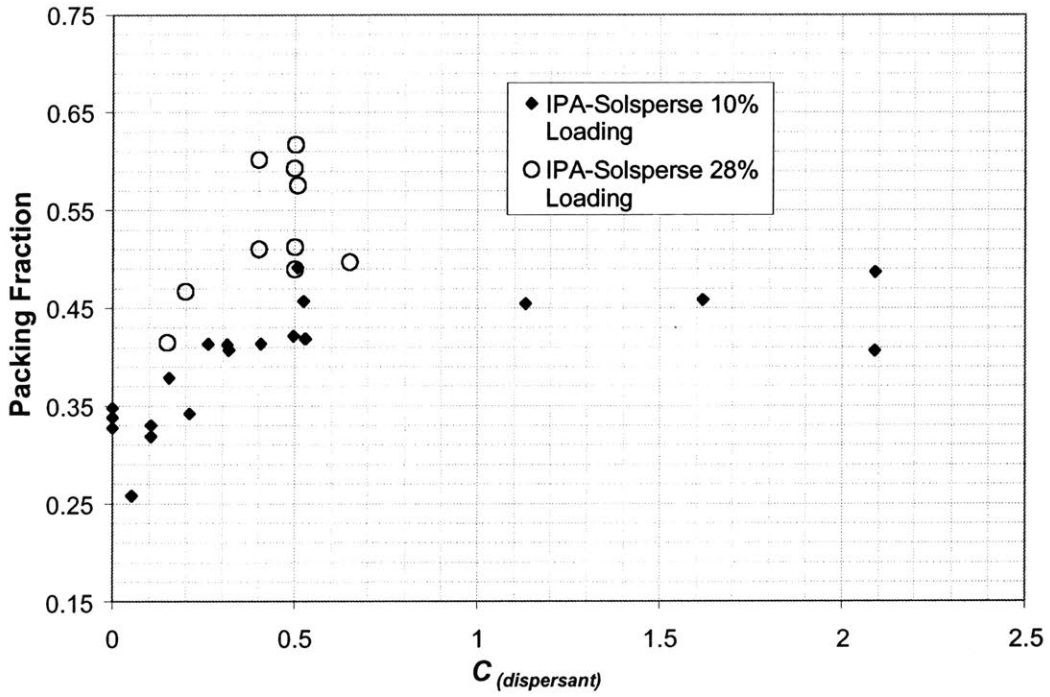

Figure 21 Sedimentation packing fractions for 10vol% and 29vol% WC-Co slurries versus dispersant concentration[17].

The packing fraction data shows a plateau for both the 10 and 28vol% solids loading slurries at a dispersant concentration of 0.5wt%, which is in agreement with the

results reported in the previous chapter with the Zephrym PD7000 dispersant. The plateau corresponds to the point above which additional dispersant no longer adsorbs to the surface of the powder. At this point a monolayer of dispersant is covering the powder particles. Little gain in packing fraction was achieved by the addition of more Solsperse above 0.5wt%. Excess dispersant may cause incomplete organic burnout of the WC-Co powder beds before sintering and leave excess carbon content. A concentration of 0.5wt% Solsperse was considered the optimum dispersant concentration.

The packing fraction for sedimented 28vol% slurries with 0.5wt% PVP were lower than for the Solsperse or Zephrym slurries of the same solids loading. The PVP slurry showed a packing fraction of 0.49, as compared to 0.52 and 0.53 for the Zephrym and Solsperse slurries, respectively. WC-Co slurries containing 0.5wt% Solsperse and 0.5, 1.1, and 1.6 wt% PEG were also tested, including a second 1.1wt% PEG slurry in which the redispersant was added prior to milling. These additions of redispersant had no measurable effect on the packing fraction.

A direct comparison of Solsperse slurries using premixed WC-Co powder and separately received WC and Co powders showed that the use of the premixed powder caused the packing fraction of the slurry to decrease significantly to 0.43. The data described above is summarized in Table 4.

Slurry Composition	Packing Fraction
0.5wt% Solsperse	0.53
0.5wt% Zephrym	0.52
0.5wt% Polyvinylpyrrolidone	0.49
0.5wt% Solsperse, Premixed WC-Co powder	0.43
0.5wt% Solsperse, 0.5wt% PEG	0.52
0.5wt% Solsperse, 1.1wt% PEG	0.52
0.5wt% Solsperse, 1.6wt% PEG	0.52
0.5wt% Solsperse, 1.1wt% PEG(added before milling)	0.52

Table 4: Effect of slurry composition on sedimentation packing fraction for a 28vol% solids loading.

The effect of milling time on the packing fraction of 28vol% WC-Co, 0.5wt% Solsperse, Zephrym, and PVP slurries is shown in Figure 22. Samples of slurry were taken after 21, 41, 65, and 113 hours of milling to record sedimentation packing fraction. The packing fraction remained relatively unchanged after 21 and 41 hours but decreased for the 65 and 113 hour samples.

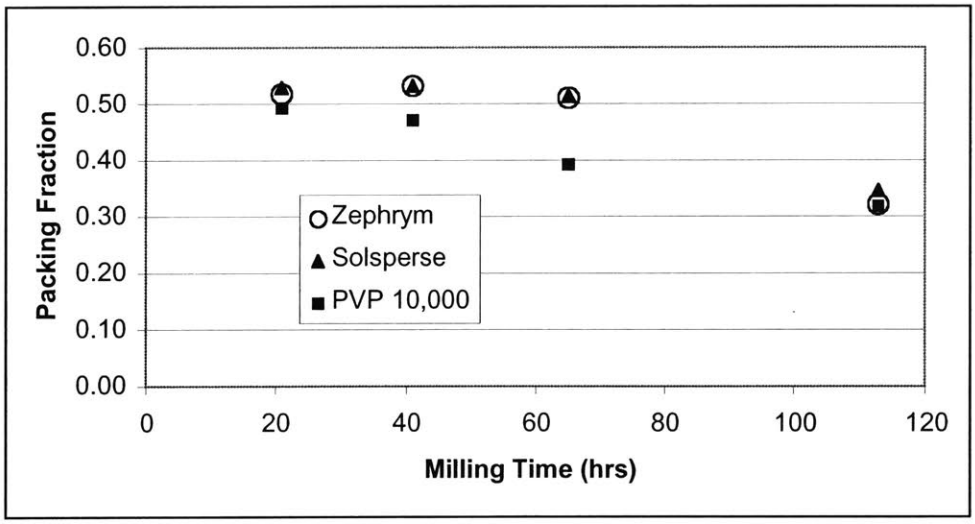

Figure 22: Effect of milling time on packing fraction of 28vol% WC-Co slurries.

3.1.3.2 Rheology

The slurry viscosity and yield stress were tested to gain a measure of the stability of the dispersion as well as a means to compare the effects of variations in materials and slurry composition.

A viscosity versus shear stress curve can take on a number of shapes. A fluid whose viscosity remains constant as the shear rate increases is known as a Newtonian fluid. However, if the viscosity decreases as the shear rate increase the fluid is said to be Shear Thinning . A fluid that has a yield stress but otherwise behaves in a Newtonian manner is called a Bingham fluid. Figure 23 illustrates the procedure for determining the yield stress of a fluid. The shear rate vs. shear stress data is plotted and the linear portion of the curve is extrapolated to the y-axis to obtain the yield stress. The presence of either shear thinning behavior or a yield stress indicates that the fluid contains a network of particles. The yield stress measures the point at which the interparticle forces of attraction are overcome and the fluid begins to flow. If the particles are not spherical

they can align themselves with the direction of the flow as the shear rate increases to create the shear thinning behavior.

28vol% solids loading WC-Co slurries were tested to determine the difference between slurries made with the Solsperse, Zephrym, and PVP 10,000 dispersants at various milling times. The effect of changing PEG concentration in Solsperse slurries was tested for slurries containing 0.5, 1.1, and 1.6wt% of the solids added after milling. Also, a second sample of slurry was made at the 1.1wt% concentration to test the effect of adding the PEG before milling. Finally, measurements were made to determine the difference between slurries made with the Solsperse dispersant and either the premixed WC-Co powder or the separately received powders.

A Paar Physica DSR4000 Universal Dynamic Spectrometer was used with the parallel plate and solvent trap attachments to measure the properties of the slurry. A plate separation of 0.25mm was needed to ensure complete filling of the gap between the plates because of the low slurry surface tension. The slurry underwent a linear ramp in shear stress to $500s^{-1}$ then it was ramped back down at the same rate in order to ensure that solvent evaporation or particle settling were not introducing very large errors into the data. Each linear ramp consisted of 30 points with a wait time of 3 seconds per point. This developed two curves, and any difference between the two is due to either solvent evaporation or particle settling. Figure 23 shows that the difference between the two curves for both viscosity and shear stress was small but not negligible.

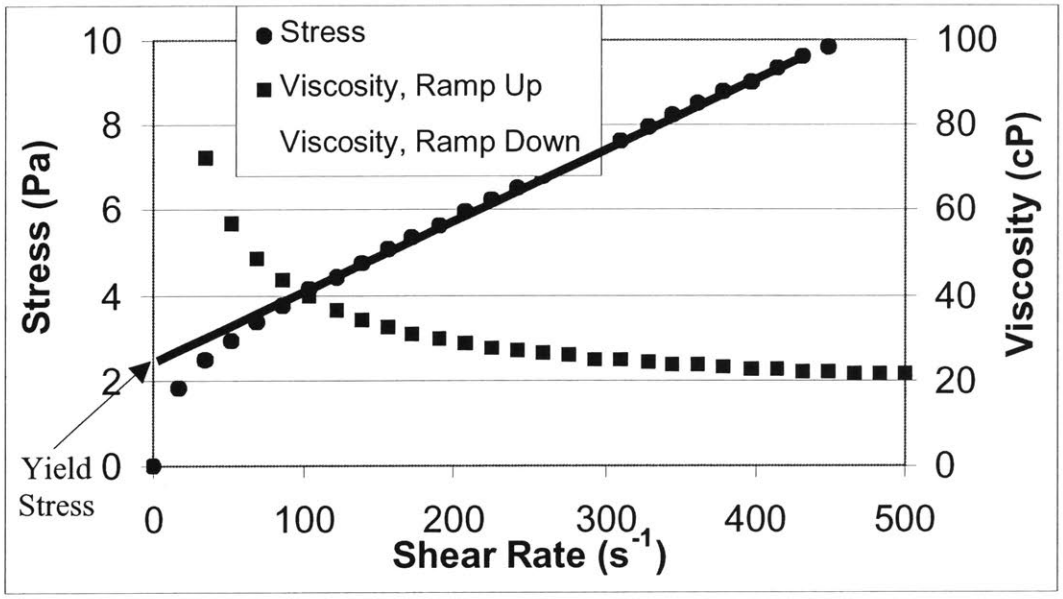

Figure 23: Rheology data for a 0.5wt% WC-Co slurry using WC and Co powders received separately.

A sample of slurry was tested at a constant shear rate of 400 s^{-1} to determine if the cause of the difference between the curves was just from drying effects. The results of the run are shown in Figure 24. The difference between the two points at a shear rate of 155s^{-1} in Figure 23 is 0.9 cP and are 123 seconds apart, which agrees with the difference of 1.1cP predicted by the drying in Figure 24.

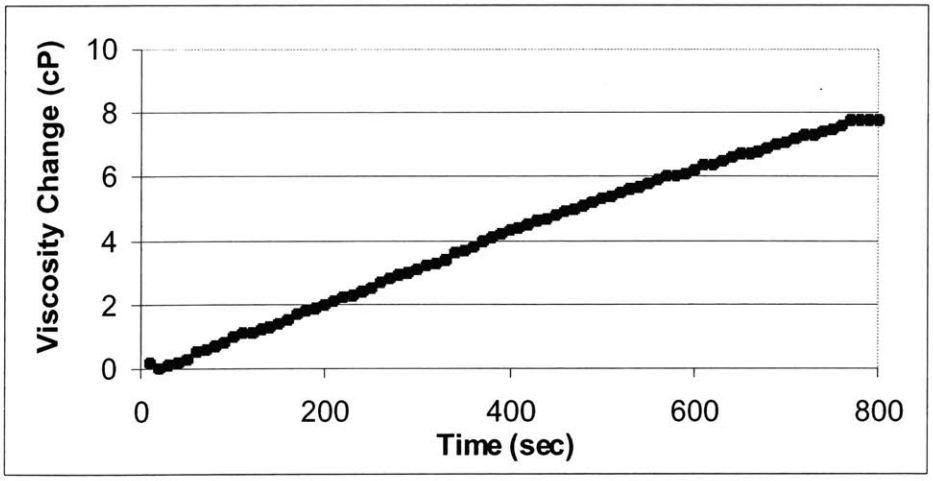

Figure 24 Change in viscosity due to drying of a 28 vol% WC-Co, 0.5wt% Solsperse slurry sheared at $400s^{-1}$

Experiments were initially conducted on premixed WC-Co powders as mentioned in the previous section. The effect of the dry mixing process can be seen by comparing the viscosity and yield stress for a slurry made with the premixed powder and one made with the WC and Co powders received separately. Table 5 contains the data for this experiment, which shows that using the premixed powders resulted in a slurry that had a much higher viscosity and yield stress. The decrease in the slurry stability with the premixed powder is believed to be a result of contamination of the powder surface with the paraffin wax used to aid the dry mixing process and the solvent used to strip the wax afterwards. Examination of pre-mixed powder reveals that it releases a strong odor that is not present in the separate powders. These contaminates prevent the dispersant from adsorbing to the powder surface. The poor solubility of paraffin wax in alcohol causes the wax to remain on the surface of the powder.

Slurry Dispersant and Redispersant Concentrations (wt% Based on Powder)	Viscosity at $400s^{-1}$ (cP)	Yield Stress (Pa)
0.5 wt% Solsperse	21.4	2.37
0.5 wt% Zephrym	21.1	2.35
0.5 wt% PVP 10,000	25	2.44
0.5 wt% Solsperse, WC-Co premixed Powder	43.5	8.01
0.5 wt% Solsperse, 0.5wt% PEG	22.2	2.31
0.5 wt% Solsperse, 1.1wt% PEG	24.0	2.44
0.5 wt% Solsperse, 1.1wt% PEG (Added before milling)	25.7	2.53
0.5 wt% Solsperse, 1.6wt% PEG	25.9	2.35

Table 5: Viscosity and yield stress data for multiple WC-Co slurry systems at 28vol% Solids loading.

Table 5 shows that the rheology data recorded for the Zephrym and Solsperse dispersants are almost identical, which further suggests that the two dispersants are chemically equivalent. The PVP dispersant had a slightly higher viscosity and yield stress than the Solsperse or Zephrym dispersants. The addition of PEG to the slurry before milling produced a slurry with only a slightly higher viscosity and yield stress.

Another factor that affects the stability of the slurry is the mix ratio of the WC and Co powders. Measurements were made of slurries containing 1.5, 3, 4.5, 6, and 10 wt% Co of the solids, as well as a WC slurry at the same solids loading. The WC slurry exhibited Newtonian behavior, with no shear thinning or yield stress. With the addition of the Co the viscosity and yield stress increased with the Co content. Co slurries were made but the viscosity curves showed strange jumps in the data. This suggested that the Co slurries were very unstable and were drying and settling too fast to be tested with the parallel plate viscometer.

a)

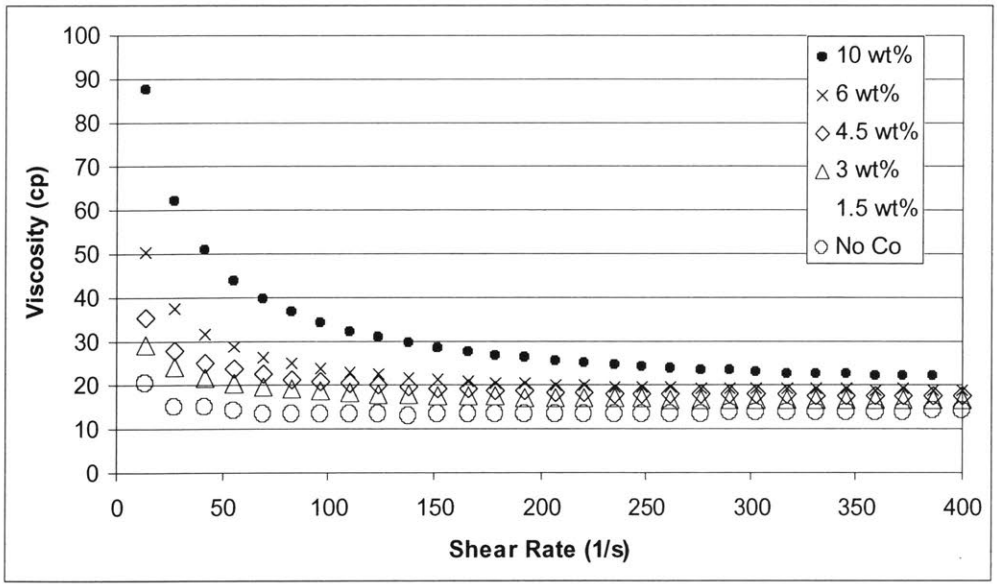

b)

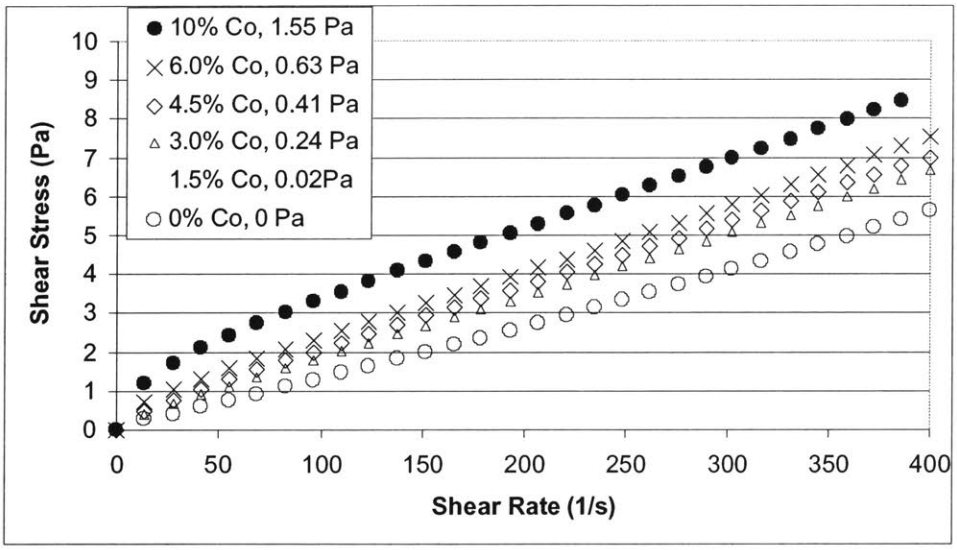

Figure 25: Viscosity data showing effect of Co content (wt% of WC-Co powder) for a 28vol% solids, 0.5wt% Solsperse slurry on a) viscosity and b) shear stress. Values reported in legend of graph (b) are yield stresses.

The effect of milling time on slurry viscosity was also measured. Three 28 vol% WC-Co slurries using 0.5 wt% of either Zephrym, Solsperse, or PVP as the dispersant were sampled after 21, 41, 65, and 113 hours of milling time. Increased milling times caused an increase in the slurry viscosity, as shown in Figure 26.

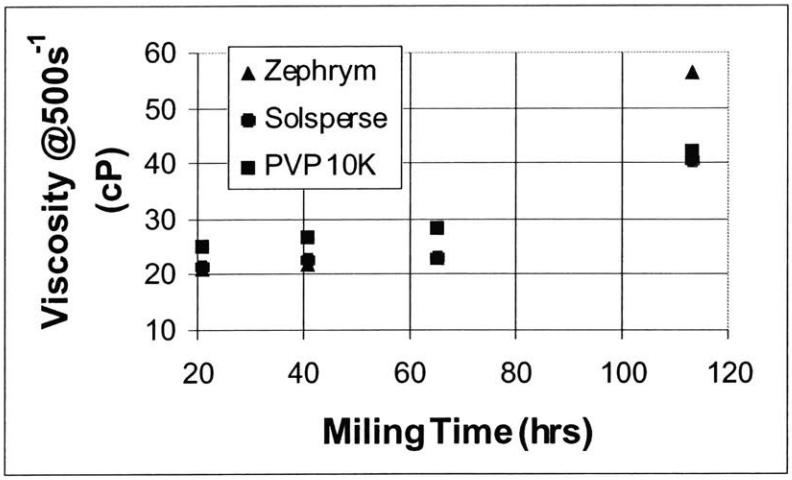

Figure 26: Affect of milling time on the viscosity of 28vol% WC-Co slurries.

3.1.3.3 Green Density and Pore Size Distribution

The green density of slip cast powder beds is reported as a percentage of the theoretical density of the WC-Co powder, which is 14.47 g/cc. The ability to sinter to full density requires that a threshold green density be reached. This lower limit is normally around 50% of the theoretical density in ceramic systems. The value of the green density provides information about the stability of the slurry system since its value can differ greatly between a dispersed and flocked slurry. Flocked slurries will not pack to a high density and will contain large pores that lower the green density and cannot be closed during sintering, as described in the previous section. These pores can act as stress concentrators while a cutting tool insert is being used and cause premature failure.

A Micromeritics Autopore II 9220 mercury intrusion porosimeter was used to measure the green density of the powder beds. A powder bed sample of known weight was placed in a container of known internal volume and weight called a penetrometer. The penetrometer and sample were then brought to a vacuum of 50μm of mercury then backfilled with liquid mercury at a pressure of 1.5 psig. The mercury does not infiltrate

the powder bed at this pressure, but will closely surround the sample since it is non-wetting it. The penetrometer, sample, and mercury were then weighed to determine the mass, and thus the volume, of mercury that filled the penetrometer. The volume of the powder bed was determined by subtracting the volume of the mercury from the volume of the penetrometer. The density of the powder bed was calculated by dividing the sample mass by its volume. The % theoretical density was then calculated by dividing the bed density by the density of the WC-Co powder.

The pore size distribution of the powder bed was measured. The filled penetrometer was placed into the high-pressure port of the porosimeter. It was subjected to a range of pressures, ramped incrementally from 30psig up to 60,000 psig. The premise of this procedure is that pressure is needed to force a non-wetting liquid into a pore to overcome the capillary pressure produced by the curvature of the liquid within the pore. The capillary pressure, and therefore the externally applied pressure, is determined by the diameter of the pore D, the pressure P, the surface tension γ and the contact angle φ in the form of Equation 3.1, which is a form of the Washburn Equation[18,19].

$$D = -(1/P)\, 4\, \gamma \cos(\varphi) \tag{3.1}$$

The porosimeter measures the amount of mercury that infiltrates into the bed at each pressure increment and converts this into a plot of cumulative volume as a function of pore diameter. A plot of incremental volume as a function of pore diameter is obtained by taking the derivative of the cumulative volume plot.

Green density values were collected to judge the performance of different slurry systems. Powder bed samples made with the Zephrym PD7000 dispersant produced similar green densities seen in the earlier work conducted by Guo and discussed in the

previous chapter. These results were obtained using the premixed WC-Co powder received from Valenite, Inc. Powder beds were also made from non premixed powders. The green density of the powder beds increased by 10%, from 44.3% to 54.2% when the slurry was formulated with the separate powders. The density of the powder beds using Solsperse and Zephrym were the same. The addition of either PPG or PEG as a redispersant after milling the slurry did not have a noticeable impact on the value of the green density, as seen in Table 6.

WC-Co Slurry System	Green Density (% Theoretical)
28 vol% Premixed Powder, 0.5wt% Zephrym Dispersant	44.3 ± 1.5%
28 vol% Separate Powders, 0.5wt% Zephrym Dispersant	54.2 ± 1.5%
28 vol%, 0.5wt% Solsperse Dispersant	55.4 ± 1.5%
28 vol%, 0.5wt% Solsperse Dispersant, 0.5wt% PPG Redispersant	56.8 ± 1.5%
28 vol%, 0.5wt% Solsperse Dispersant, 1.1wt% PEG Redispersant	56.2 ± 1.5%
28 vol%, 0.5wt% Solsperse Dispersant, 1.6wt% PEG Redispersant	55.2 ± 1.5%
28 vol%, 0.5wt% Solsperse Dispersant, 0.5wt% PEG Redispersant with BHT Antioxidant	54.0 ± 1.5%
24 vol%, 0.5wt% PVP Dispersant, 0.6wt% PEG Redispersant	49.5 ± 1.5%

Table 6: Table of Green Density values for multiple slurry systems

The results for the pore size distribution showed a narrow range, centered on 0.2μm in diameter for Solsperse beds and 0.3μm for PVP beds. These results are shown in Figure 27.

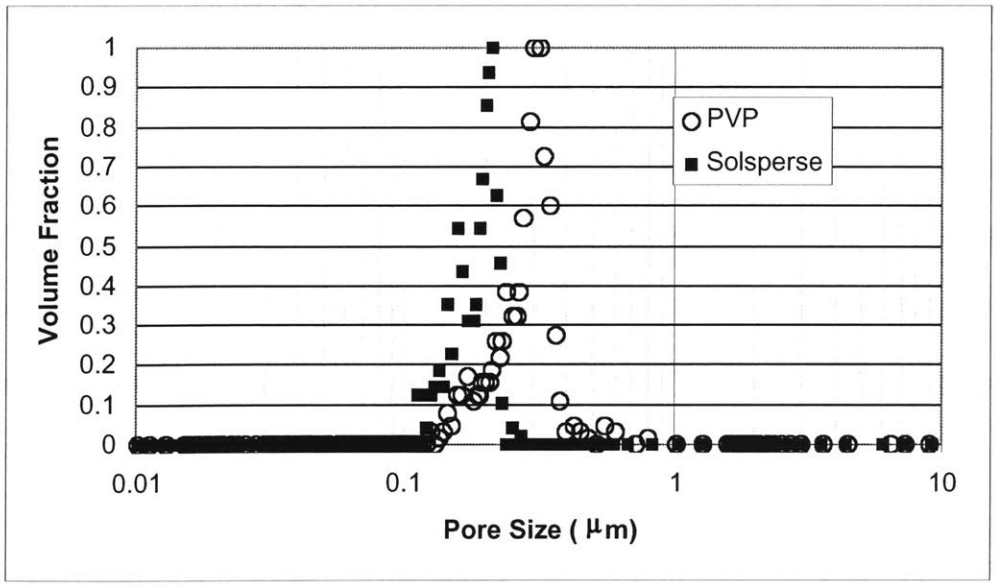

Figure 27: Pore size distribution of WC-Co powder beds showing cumulative and incremental volume fractions.

3.2 Binder Systems

Multiple binder materials were tested with the WC-Co powder beds. Poly(acrylic acid) (PAA), Cyanoacrylate (CA) glues, Poly(vinyl acetate) (PVAc), and Polyethylenimine (PEI). The binders act to glue the particles together in the regions they are deposited in. The binders are examples of three different mechanisms that can be used as a binder system. The PAA and PEI are thermally cured after printing to form an insoluble network to hold the powder particles together during redispersion, while the CA cures when it comes into contact with air, and the PVAc precipitates as the solvent it was dissolved in dries. These systems will be discussed further in the following sections.

3.2.1 Poly(Acrylic Acid)

Initially, the primary binder material selected for testing with the WC-Co slurry was a Poly (acrylic acid) (PAA) (MW 60000) solution with a glycerol crosslinking agent.

The glycerol added was 10wt% of the amount of PAA in the solution. Both water and ethanol were used as a solvent for the PAA binder solution. The PAA was obtained from Acumer 1510 (Rhom and Haas), which is a 25.2 wt% PAA — Water solution. For the aqueous binder solutions the Acumer was diluted to the test concentration, but for the ethanol solutions all the water was removed from the Acumer first. This was done by heating it to 50°C in a vacuum oven overnight. This removed the water and the PAA was left as a solid to be dissolved in the ethanol.

The PAA acted as a binder only after it was cured in an oven at 150°C for 1hr in an argon atmosphere. The reaction that takes place during the cure step is shown in Figure 28[5]. After this step the PAA forms an insoluble polymer network around the particles in the powder bed.

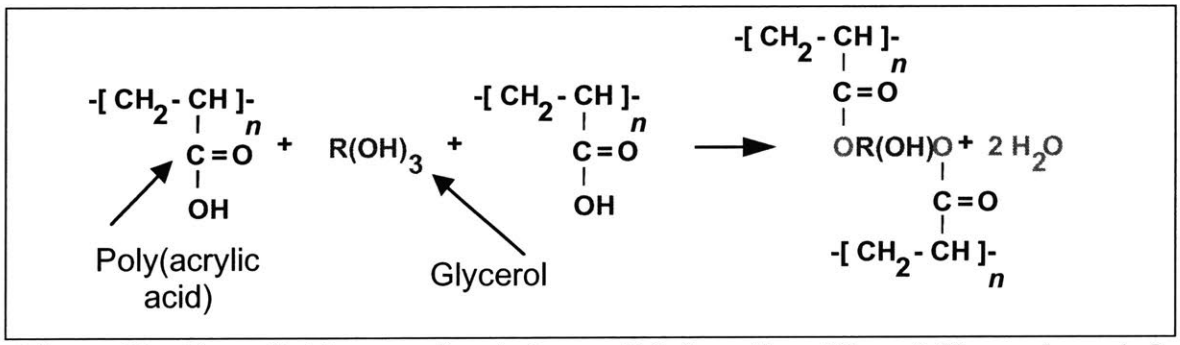

Figure 28: Cross-linking reaction between Poly(acrylic acid) and Glycerol carried out at 150°C in and argon atmosphere[5].

An isotherm for the adsorption of PAA onto the surface of the WC powder was created using a Beckman DU 640 Spectrophotometer to measure UV absorption. Aqueous solutions of PAA were formulated with concentrations of 5, 1.5, and 0.75 vol%. These solutions were then mixed with the WC powder to form at 20vol% solids loaded slurry. The slurries were then rolled without media on a ball mill for 19hrs to allow the polymer adsorption to equilibrate. The slurries were centrifuged for 30 minutes at

1,150G (1,150 x gravity) after rolling, then the supernatant was taken and centrifuged again for 60 min at 12,000G. A 20 vol% WC slurry without PAA was also created and rolled for 19hrs in order to determine a baseline UV adsorption for the dissolved tungsten, shown in Figure 29. The scan showed that the dissolved species from the WC powder strongly adsorbed in the UV region of interest. This baseline was then corrected for dilution and subtracted from later absorption curves in order to obtain the amount absorbed solely by the PAA.

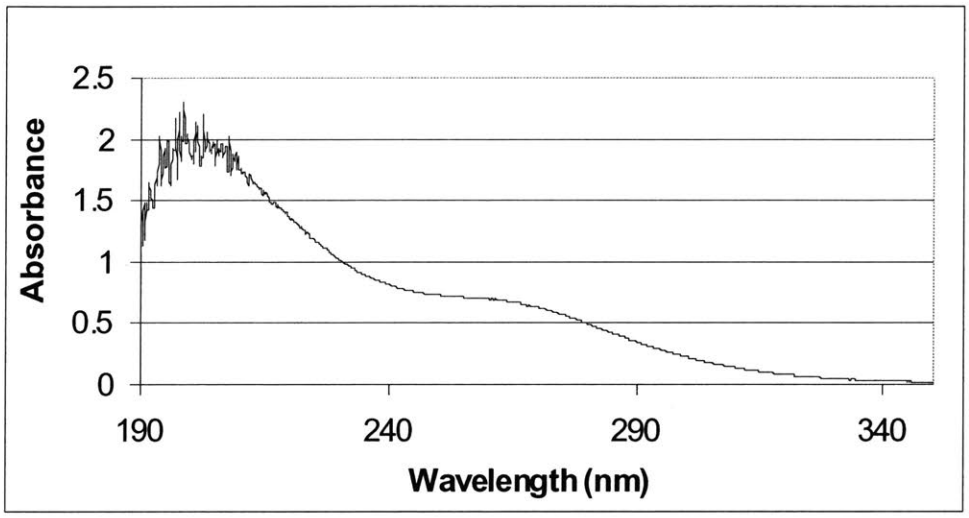

Figure 29 UV absorption of supernatant from a 20vol% WC aqueous slurry, diluted 50:1.

A calibration of UV absorption versus PAA concentration was created by using 0.01, 0.05, and 0.1vol% PAA solutions and is shown in Figure 30. Absorption values were recorded at a wavelength of 211nm, which is the location of an absorption peak for PAA. The 5, 1.5, and 0.75 vol% PAA supernatants were diluted 100:1, 100:1, and 75:1, respectively, in order to lower the UV absorption value to within the detection limits of the machine. The values of absorption for the slurry supernatants were compared to the concentration-absorption calibration curve, after correction for the tungsten absorption, to

obtain the concentration of PAA left in the liquid. This concentration was then compared to the original concentration of PAA. Any decrease in this concentration is due to PAA adsorbing to the surface of the WC powder and provides the mass of PAA adsorbed the powder surface. The results were plotted in Figure 31 to show how the equilibrium concentration of PAA adsorbed to the surface of the WC changed with the concentration of the solution.

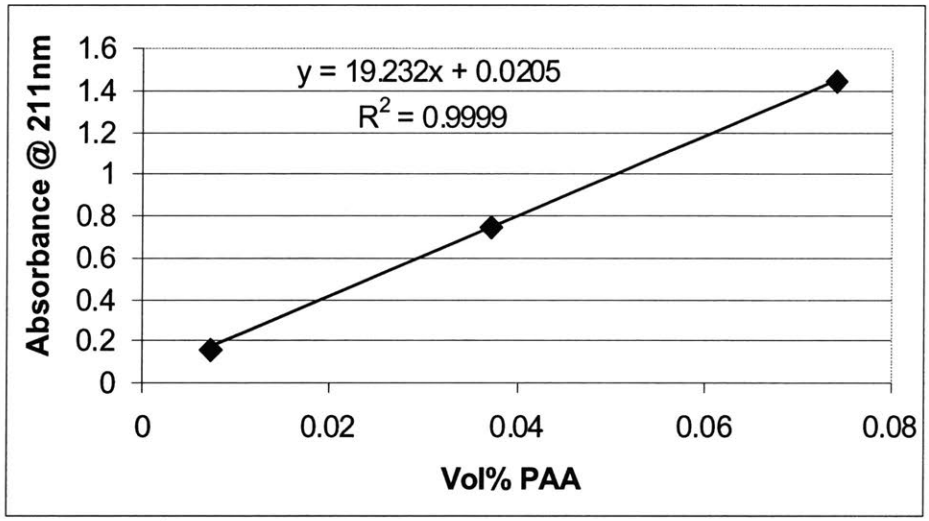

Figure 30: Calibration curve of PAA absorption at 211nm.

Figure 31 shows the results obtained with WC as well as results of the same test performed by Holman[12] for alumina, titania and silica. The negative adsorption values were a result of the dissolved tungsten in the supernatants absorbing UV radiation. This happens if the tungsten ions are present at a higher concentration in the supernatants containing PAA than the supernatant used as a baseline for tungsten absorption. It was observed that the solutions were a clear yellow color, which were progressively darker with increasing PAA concentration. This indicated that there was more dissolution of the WC powder in the solutions containing PAA than in the baseline solution.

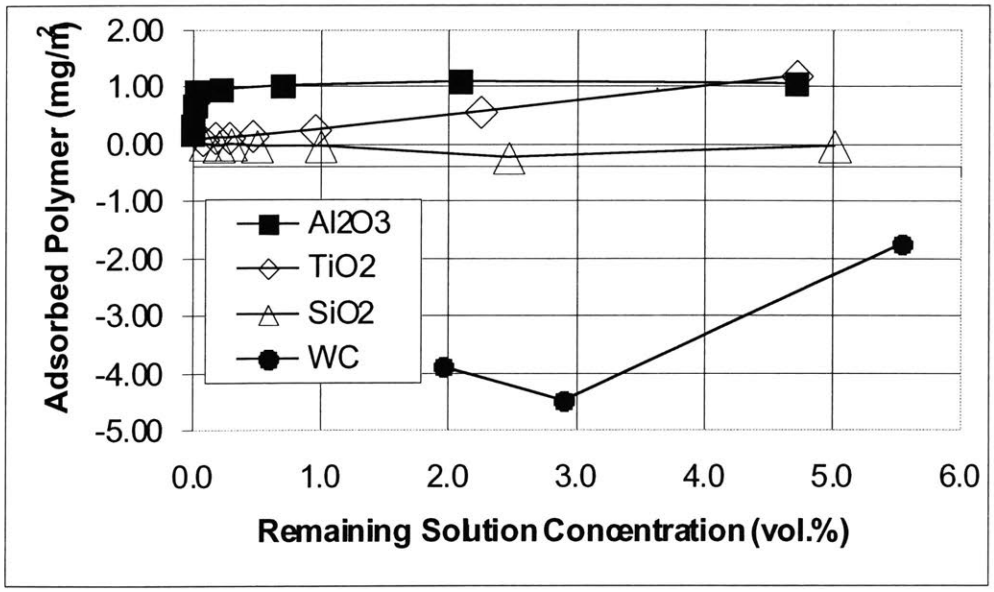

Figure 31: Adsorption of PAA onto the surface of ceramic powders.

The pH values of the 5, 0.3, and 0.0 vol% PAA supernatants were measured and were 2.14, 2.92, and 3.1, respectively.

3.2.2 Cyanoacrylate

Tests to determine the effectiveness of a Cyanoacrylate binder, more commonly known by the trade name Super Glue were facilitated by the need to develop a binder system that did not require a thermal curing step in order to be used with the powder beds containing Solsperse dispersant. The trade name Super Glue, although generally used to describe all cyanoacrylate glues, is actually the ethyl ester of cyanoacrylate and is designed to bond better to plastics. Conversely, the methyl ester is designed to bond better to metals. Figure 32 shows the chemical structures of both esters.

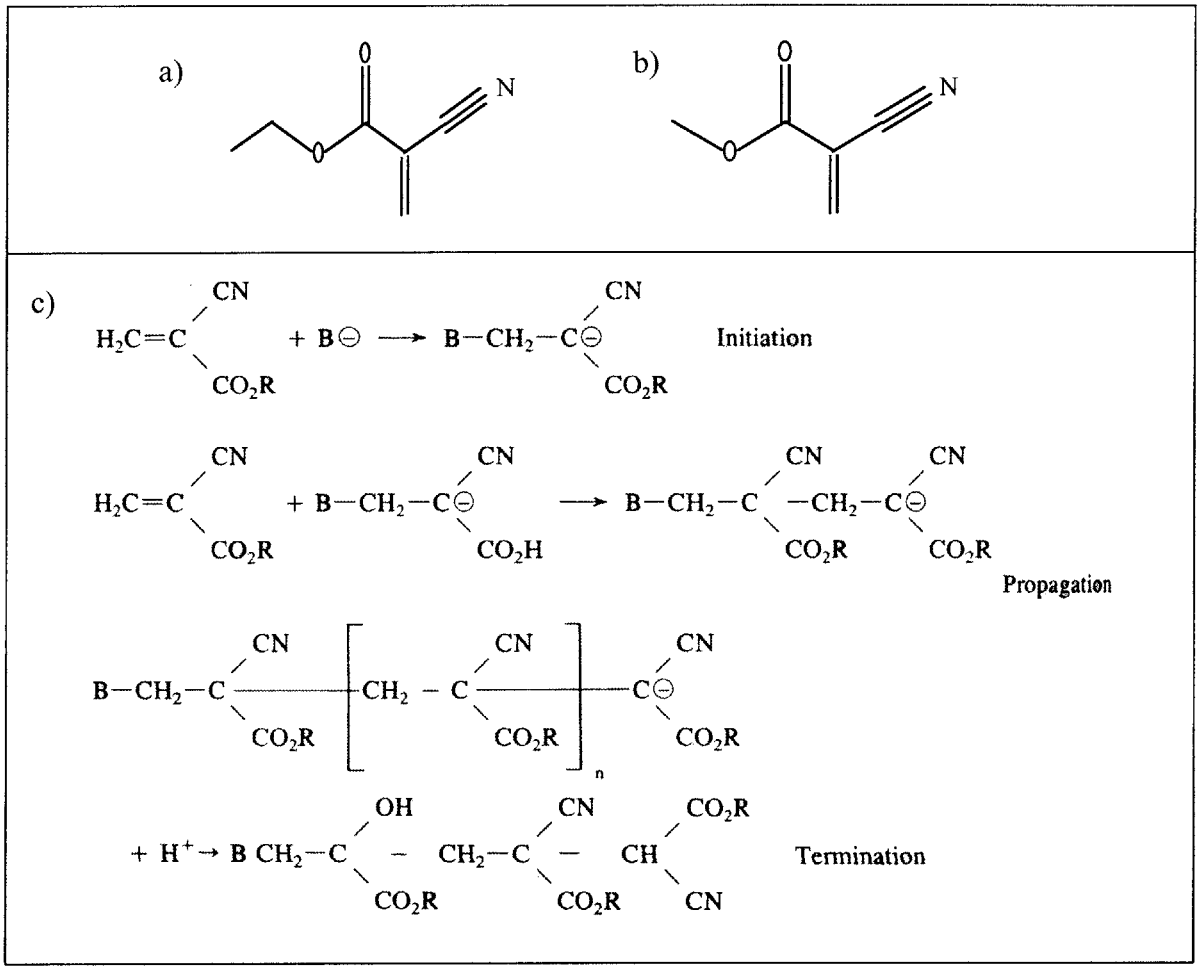

Figure 32: a) Chemical structure of the ethyl and b) methyl esters of cyanoacrylate. c) Reaction mechanism of CA glues[20].

Cyanoacrylate adhesives polymerize rapidly by an anionic mechanism in the presence of a weak base, such as alcohol or water. The C-C double bond in the structure is highly reactive due to the nearby —CN and —COOR bonds. The curing reaction is shown in Figure 32c. The CA glues can also polymerize by a free radical mechanism. The steps of the mechanism are identical to the anionic mechanism shown above when the [B^-] anion is replaced with a [R^*] free radical, and when the [H^+] proton is replaced by another [R^*] radical for the termination reaction. The anionic mechanism is strongly favored over the free radical mechanism, however. This preference for the anionic

mechanism proves useful since the shelf life of the CA glue can be extended by the addition of large amounts of free radical stabilizers, such as hydroquinone, without adversely affecting the cure properties[20].

The brands of CA glues tested were Permabond 910, Holdtite CA20, and Loctite 401, 406, 430, 493, and 495. The chemical composition of these glues is shown in Table 7.

CA Brand	Ester Type	Additive Composition
Holdtite CA20	Ethyl	None
Permabond 910	Methyl	None
Loctite 493	Methyl	0.1-0.5% Hydroquinone
Loctite 430	Methyl	0.1-0.5% Hydroquinone, 5-10% PMMA
Loctite 495	Ethyl	0.1-0.5% Hydroquinone, 3-5% PMMA
Loctite 406	Ethyl	0.1-0.5% Hydroquinone, 1-3% PMMA
Loctite 401	Ethyl	0.1-0.5% Hydroquinone, 5-10% PMMA

Table 7: Chemical composition of CA glues tested.

3μl droplets of CA samples were placed onto two WC-Co powder beds to test the superglues. The first bed contained 0.5wt% Solsperse and 1.1 wt% PEG, and the second contained 0.5wt% Solsperse. The CA samples were tested as received, in 50wt% solutions of CA in acetone, and in 10wt% acetone solutions.

Test results showed that none of the as received glues or the 50wt% solutions infiltrated into the powder beds. Possible reasons for this are the viscosity was too high, the surface tension did not allow the glue to wet the powder bed, or by rapid polymerization forming an impermeable film at the powder bed surface. The best results

were obtained with newly made 10wt% solutions of Holdtite CA20 and Permabond 910, which infiltrated the powder beds and formed droplet primitives. The solutions did not fully infiltrate into the beds after aging for 30 minutes. This was evident by a darkened ring left on the surface of the powder bed. The Loctite glues showed a wide variety of infiltration behaviors with the 10wt% Loctite 493 solution showing the best results. However the 493 still left a ring of CA film on the top of the bed. The rest of the 10wt% solutions of Loctite glues either left a small amount of film behind, like the 493, or did not infiltrate at all, like the 401. Figure 33 shows the results of the infiltration testing.

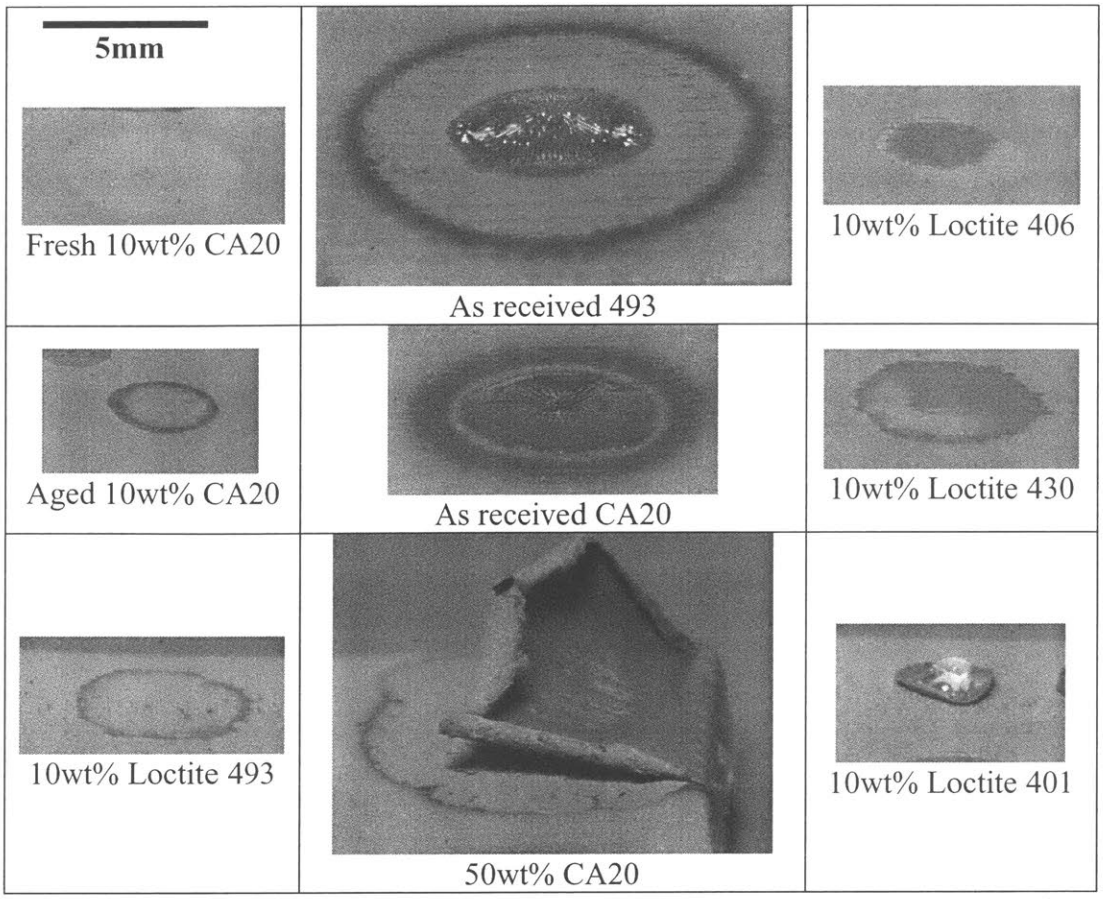

Figure 33: Images of infiltration behavior of 3µl droplets of CA samples into WC-Co powder beds. All images at same scale.

Droplets formed from the as received glues and the 50wt% solution shows evidence of blooming in the figure above. This is the industry term for the discoloration caused by the condensation of CA vapors onto the object being glued.

It was observed that the CA glues began to polymerize upon the addition of the acetone, with different behavior seen for the methyl and ethyl esters. The viscosity of the ethyl ester solutions increased over time. The solutions of the methyl esters, however, remained at a low viscosity but became cloudy white.

The use of cyanoacrylate binders was not tested further due to the problems that this system brought to the printing process. The use of acetone as a solvent requires the use of a fume hood during printing because of its toxicity and high volatility. Also,

acetone attacks and swells many plastics, limiting the selection of materials that a printhead could be designed with. Another factor against the use of cyanoacrylate is that if the fast drying binder solidifies on the printhead when the operation is stopped it forms and insoluble clog, which may not be able to be removed. Thus the whole printhead needs to be discarded. Finally, the reaction of the CA glues with the acetone occurs rapidly, on the order of minutes. This excludes the system from use with 3DP because the time that the solution needs to be stable over is on the order of hours.

3.2.3 Poly(Vinyl Acetate)

PVAc was tested in order to develop a system that did not require a thermal cure step, like the CA glues. The PVAc was acquired from Sigma-Aldrich and has an average molecular weight of 85,000. The key properties of this polymer were that it is a solid at room temperature and is soluble in methanol but not in water. These properties were necessary for the development of a new S-3DP system where printed WC-Co powder beds redispersed in water. The solubility of PVAc in alcohol was not required, but the use of alcohol over other more toxic solvents was favorable.

Similar to the tests with the CA glues, 3 μl droplets of a 3.5vol% PVAc were placed onto WC-Co powder beds containing only the Solsperse dispersant to determine if the binder solution infiltrated and formed a droplet primitive. Tests confirmed that the solution did infiltrate, but the droplet primitives were weak. 0.01-inch PVAc films were made by spreading a viscous 30vol% PVAc-MeOH solution onto a rubber substrate to determine the cause of the weakness. The resulting PVAc film was then pealed from the rubber when the MeOH evaporated from the solution. The films produced were brittle, strong, insoluble in water and required 1.5 days for any signs of swelling to appear.

Next, the same PVAc solution was used to mix PVAc and Solsperse in a 1:2 volume ratio. This is the same ratio of PVAc to Solsperse that is found in the pore space of a powder bed. A precipitate was formed indicating that the Solsperse and PVAc reacted upon mixing. The precipitate was tested and found to be insoluble in methanol but soluble in water. Testing of PVAc as a binder for powder beds made with Solsperse as a dispersant was ended for this reason.

3.2.4 Polyethylenimine

Polyethylenimine (PEI) with a molecular weight of 10,000 was obtained from Polysciences Inc. The polymer structure, shown in Figure 34, consists of a main chain of ethylenimine mer units, with branches every 3 to 3.5 nitrogen atoms. The nitrogen groups become protanated in an aqueous solution and the PEI acquires a positive charge. The positively charged PEI molecule are attracted to the negatively charged surface of the WC particles, enhancing adsorption and adhesion through a possible chemical linkage of the nitrogen groups to the surface hydroxyls of the powder.

PEI binder containing glycerol was observed to form an insoluble binder upon heating in a WC-Co powder bed. Parts made with this binder remained strong after being placed in water. Parts made with PEI binder that did not contain glycerol were became weak when they were placed in water after a curing step.

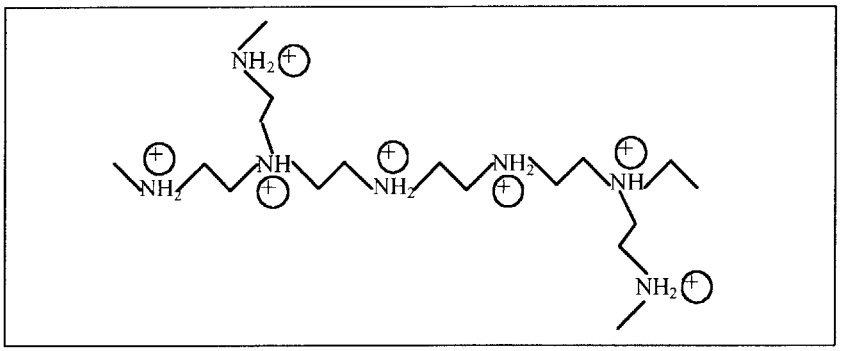

Figure 34: Branched PEI structure

The adsorption behavior of PEI on the surface of WC was measured and plotted. Aqueous solutions containing 5, 2.25, 0.75, and 0.3 vol% PEI were formulated and WC powder was added to create 20vol% solids loaded slurries. The slurries were rolled without media on a ball mill for 19 hours then centrifuged at 1,150G for 30 minutes. The supernatant was then removed and centrifuged again at 12,000G for 60 minutes. Next, the supernatant was removed again and shipped to Huffman laboratories for Kjeldahl nitrogen analysis. The supernatant from a 20 vol% WC-Water slurry as well as 3 calibration samples of known PEI concentration were also sent. The Kjeldahl analysis recorded the weight % of nitrogen in each supernatant sample. This value was used to calculate the concentration of PEI knowing that nitrogen is 31.78wt% of the PEI molecule. The concentration of PEI in the slurry supernatant was compared to the concentration before the addition of WC powder. The difference in the concentrations was caused by the adsorption of polymer to the surface of the powder. The mass of polymer adsorbed per unit area of powder was plotted on the abscissa and the concentration of PEI that remained in solution was plotted on the ordinate of Figure 35.

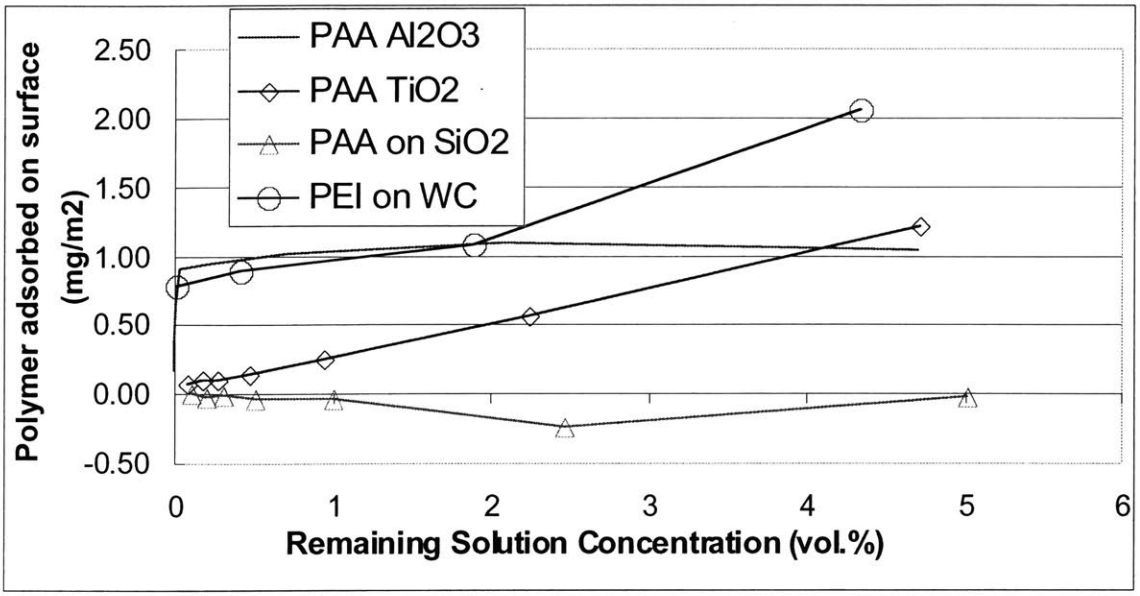

Figure 35 Adsorption isotherm for PEI on WC powder in water compared with adsorption for PAA on other powders.

The results show that the PEI was strongly adsorbed to the surface of the WC powder. The solutions appeared clear-yellow after centrifuging, and lighter in color than the WC-Water supernatant with no PEI. The yellow color grew darker from the as the PEI concentration decreased from the 5 to the 0.75 vol% PEI supernatant, but the 0.3 vol% PEI supernatant was clear and colorless. The pH values of the 5, 2.25. 0.75, 0.3, and 0 vol% PEI samples were recorded to be 10.2, 9.7, 8.6, 8.1, and 3.2, respectively.

4 3DP™ Processing Techniques

This chapter focuses on the procedures employed with the printing of WC-Co. The key factors that affect the reliability of the slurry delivery systems are discussed first, followed by the different binder printing methods and then redispersion. Results for each printing method are presented in terms of printed part resolution and sintered characteristics such as final density and pore rating.

4.1 Slurry Delivery System

The development of a slurry handling system played a key role in the experiments performed with the WC-Co system. It was necessary to develop a system that was sealed from the atmosphere and had low slurry residence times due to the high evaporation and settling rates of the slurry. Drying of the slurry while jetting causes agglomerates to form. These agglomerates travel to the nozzle and clog it or build up in the system causing changes in the flow rate. There is no control of the jetted layer height if there is no control over the slurry flow rate. Settling of particles in the slurry causes the same problems. Sediment accumulated in stagnant flow areas change the slurry flow rate over time or become dislodged and clog the slurry nozzle. Furthermore, a source of constant pressure was needed in order to jet the slurry at a uniform flow rate through the nozzle without any pressure pulses. Pressure pulses can result in slurry lines of non-uniform width being deposited on a powder bed. This non-uniformity adversely impacts the smoothness of the surface of a jetted bed and provides a means of creating voids in the bed as well. All of these problems needed to be overcome to create a stable jetting

process in order to experiment with other variables, such as binder infiltration behavior. Figure 36 shows a diagram of the systems used.

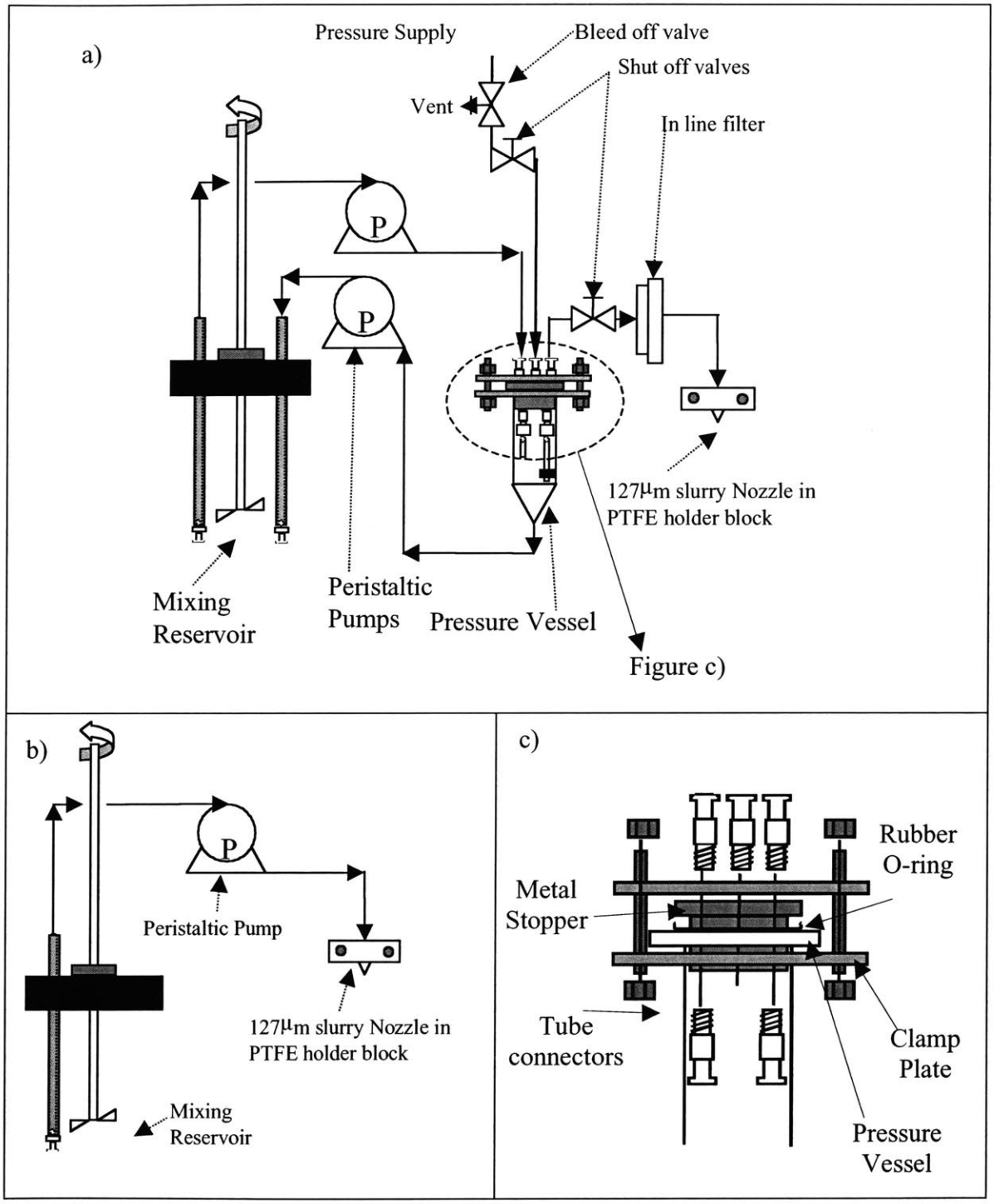

Figure 36: Diagram of slurry delivery systems. With pressure vessel a) and without pressure vessel b). Exploded view of pressure vessel and clamp c)

A mixing rod was added in order to overcome the problem of slurry settling in the main holding reservoir. A magnetic stirrer was not used since the Co particles are magnetic and were drawn to it. To overcome the problem of settling in the tubing, residence times of the slurry were calculated for a given length of tubing at varying diameters. Tubing diameters were chosen for which the residence time was less than the time it took for slurry to settle a distance equal to the diameter of the line, as calculated by Stokes settling. A recycle loop needed to be used in order overcome settling in the pressure vessel shown in Figure 36a. The peristaltic pumps were able to be operated at high speed with this configuration, which allowed the tubing used in the loop to be as large as 1/16 diameter. The tubing shown in Figure 36 located after the pressure vessel needed to have an inner diameter of 0.022 in order to avoid settling due to the low slurry flow rates used during a print run, while minimizing pressure loss. Connectors for lines with this small of an inner diameter needed to be made of stainless steel tubing with an outer diameter slightly larger than the I.D. of the tubing. The ends of the tubing were chamfered in order to ensure a smooth transition for the fluid flow and remove areas where powder particles built up to form agglomerates.

The primary areas of concern when attempting to seal the delivery system were at the mixing reservoir and pressure vessel shown in Figure 36a. The mixing reservoir was sealed by affixing a rubber membrane to the cover and cutting a hole slightly smaller than the stirring rod. The seal was not good enough to allow the mixing reservoir to be used as a pressure vessel although it minimized evaporation. A clamp provided a good seal and allowed the pressure vessel to be used up to 30psi.

A second slurry system was tested in order to minimize the length of tubing used as well as the number of connections used. Figure 36b illustrates the simplified slurry system. A Cole Parmer LC 7519-20 Reduced-Pulsation Cartridge Pump Head with 8 rollers and the capability to run multiple lines simultaneously was selected in an attempt to minimize the pressure pulses caused by the peristaltic pump. A single 0.022 I.D. teflon line from the reservoir was diverted into two 0.03 I.D. Masterflex tubing lines for the slurry line. These lines were passed through the pump and configured out of phase in order to minimize pressure pulses. The two lines were then merged back into a 0.022 teflon line after the pump. Initial tests showed that the slurry flow rate was not steady due to the pressure pulses formed by the pump. The use of a longer slurry line section after the pump helped to dampen the pulses through viscous losses.

Attempts to have on-off slurry control during printing proved unsuccessful. On-Off control attempts to conserve material by stopping the slurry jet when it is not being used to form a powder bed layer. Success with this type of procedure was attained with an aqueous WC-Co_3O_4 slurry system in which on-off control was used reliably during a 6 hour print run.

The increased sensitivity of the alcohol system to air leaks and other effects that cause drying is attributed to the volatility of the alcohol medium. When drying occurs in slurries there is no longer a barrier to the powder particles to overcome the Van derWaals forces between them and they come into contact. Once in contact DLVO theory predicts that it takes a very large amount of energy to separate them, which mixing does not provide. Once an agglomerate forms in the slurry system it stays, and if it is not caught by the in-line filter it goes on to clog the nozzle.

4.2 Powder Bed formation

Two methods were used to form powder beds. The first method used the conventional raster scan, which had an inter-arrival time for subsequent slurry lines that was on the order of 1 second. This is much longer than time it takes a single slurry line to slip cast. The second method used the slurry line merging station. The slurry line merging station incorporates a novel machine design that can achieve much lower inter-arrival times of approximately 25 msec[21], which is on the order of the time for a single slurry line to slip cast. The next two sections will describe these powder bed formation methods.

4.2.1 Conventional Raster

Both slurry-handling systems described above were used with the conventional raster technique. The inter-arrival time of the individual slurry lines is much longer than their slip casting times, as mentioned above. Figure 37 shows the slip casting of a single slurry line being deposited in a WC-Co bed. The powder bed was backlit in order to use the glare off the top of a wet line to determine when the line was done casting. The video recorded images at a rate of 30 frames per second. The slurry line has just been deposited in the first image. The glare off the top of the line can still be seen indicating that the line has not fully cast yet in the second image, but is not present in the third image. The images show that the slip casting time is on the order of 0.03 sec.

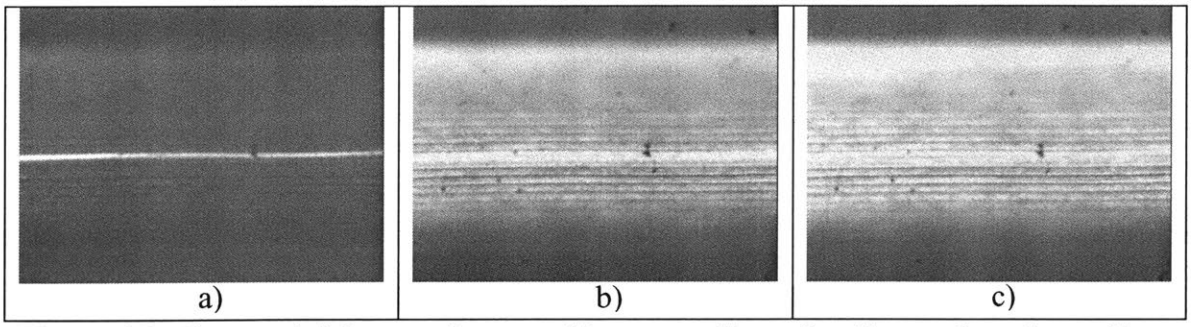

Figure 37: Sequential frames from a video recording of a slip casting slurry line. Frame rate was 30fps.

The effect of varying the line spacing of the slurry lines can be seen in Figure 38. Line pairing can be seen when the slurry line spacing is set at 400μm, but is not present for 200μm for a slurry flow rate that creates a slurry line width of 480μm. This agrees with the finding by Guo[22] that an overlap factor between the line spacing and the slurry line width of 2 was needed to avoid over saturation or line pairing.

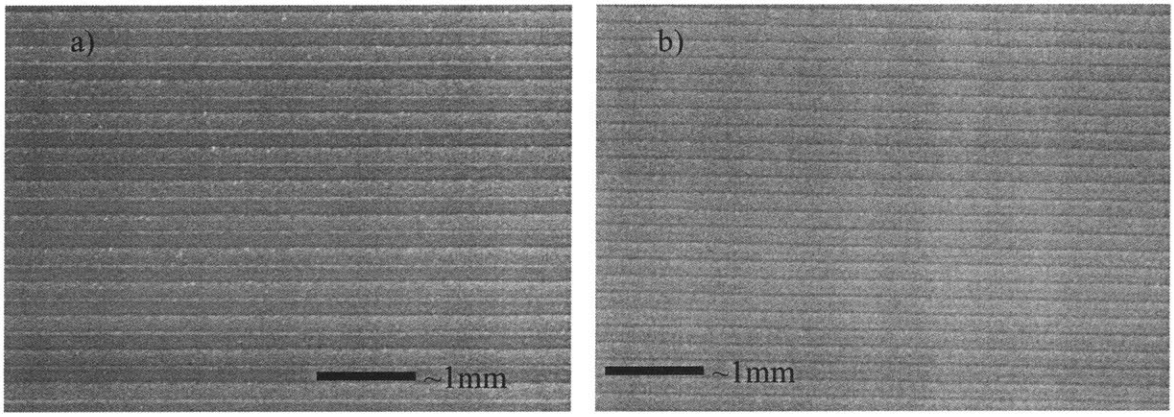

Figure 38: Effect of line spacing on powder bed surface finish a)400 μm LS with line pairing and b) 200 μm LS with no line pairing. Slurry line width was 483 μm.

The individual lines do not stack side by side for the 200μm line spacing. Instead, the lines piggy-back one on top of the next to form a continuous layer across the bed. The surface roughness formed with this effect is shown in Figure 39.

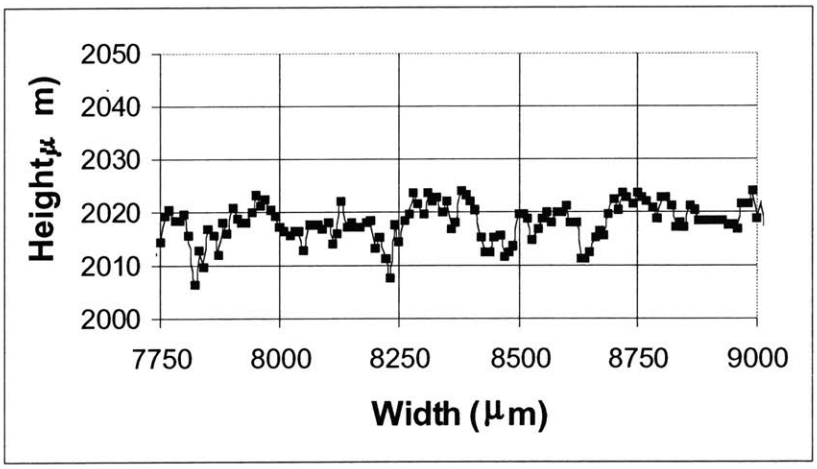

Figure 39 Surface roughness of WC-Co powder bed with a 200μm LS and a standard deviation of 3.3μm measured by laser profilometry. 35um LH.

The peristaltic pump system for slurry delivery, described above, introduced some pulsing in the flow rate of the slurry. The affect of this pulsing can be seen in Figure 40, in which slurry lines were deposited on top of two powder beds at a width sufficient to observe their individual character. Comparison of the images in Figure 40 shows that the slurry lines created using a peristaltic pump do not have as constant a width, either along a single line or from one line to the next, as lines deposited using a pressure vessel. Further work is required to fine-tune the peristaltic pump system in order to eliminate pressure pulses. One method to accomplish this is to use a longer slurry line length after the pump, in order to use viscous losses to dampen the pulses.

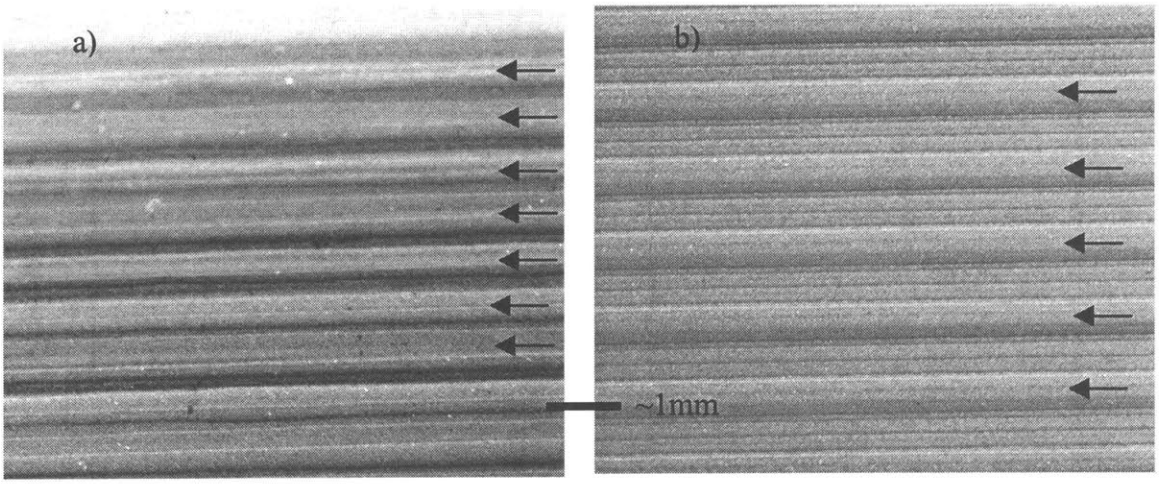

Figure 40: Comparison of individual slurry lines created with a) peristaltic pump and b) pressure vessel slurry delivery systems. Arrows indicate centerline placement of individual slurry lines.

4.2.1.1 Sintering of Conventionally Rastered Powder Beds

Samples of jetted powder beds were sintered at both Kennemetal and Valenite through a proprietary sintering schedule. The schedule included a burnout step prior to sintering in order to remove the organic content introduced by the dispersant and redispersant. Powder beds were made that sintered to full density with an acceptable porosity rating of A01-B00-C00, as shown in Figure 41. A region of powder bed with large voids is visible at the bottom of the image. This region is called the "Foundation Layers" region. In these first few layers of the powder bed the conditions of slip casting were changed due to the presence of the porous glass substrate. Observation during the deposition of these layers showed that the slip casting time was longer here. Also visible during observation were changes in color hues at the top of the first 2-3 layers, suggesting that polymer was segregating to the top of each layer.

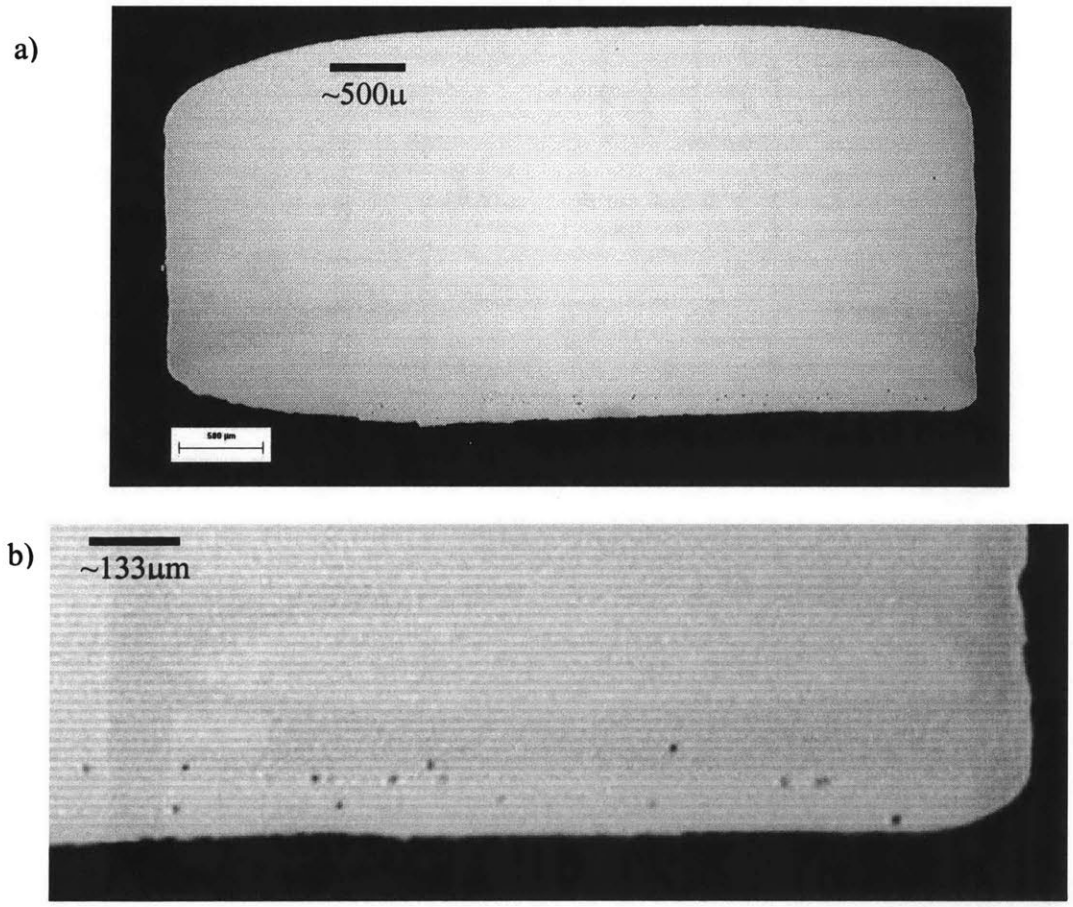

Figure 41: Cross sectional view of sintered WC-Co powder bed from Valenite with porosity rating of A01-B00-C00. LS=200µm, LH=35µm A). Close up view of foundation layers B)

4.2.2 Line Merging

The line merging method of powder formation, as mentioned above, allows for much lower inter arrival times for individual slurry lines through machine design. The decrease in inter arrival time is accompanied by high g-forces when the travel direction of the slurry nozzle is reversed. Observations of slurry deposited with this machine have shown that the g-forces can induce large pressure pulses in the slurry flow rate. The WC-Co slurry was jetted on the line merging station with the peristaltic pump setup. Figure 42 shows and image of the top of a powder bed formed with this method. It was

observed that for the slurry used, the slurry lines were slip casting faster than the inter arrival time of the lines.

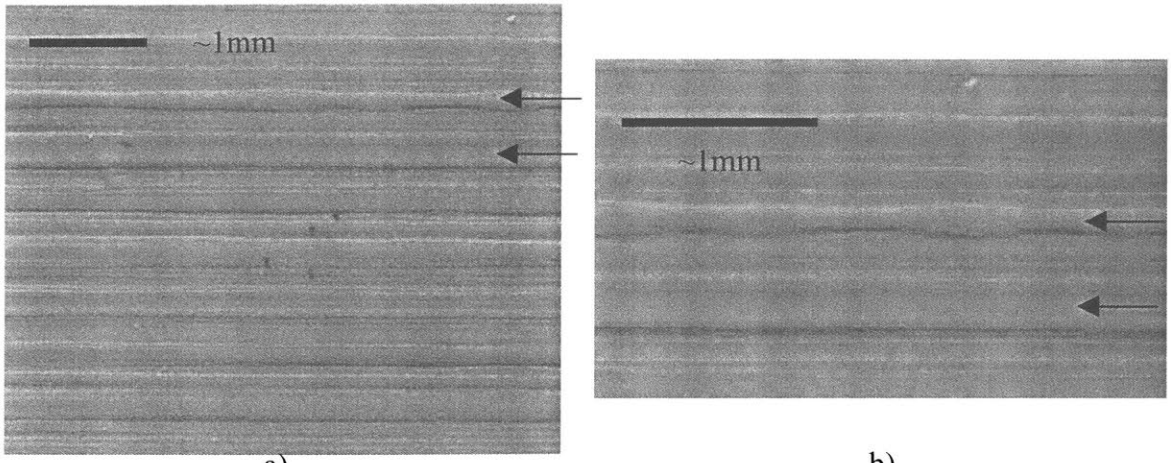

Figure 42: Surface of powder bed jetted with slurry line merging station a). Close up of two slurry lines b). Arrows indicate same lines.

The surface of the bed looked rough in the direction perpendicular to the slurry lines, as is evident in the above picture. The pressure pulses produced in the turnaround of the slurry nozzle path caused inconsistencies in the slurry line width that were worse than those introduced by the peristaltic pump alone along the length of the individual slurry lines. This can be seen by comparing Figure 40a with Figure 42. The surface roughness of a WC-Co bed formed on the line merging station was measured using a laser profilometer. Comparing the results shown in Figure 43 with Figure 39 shows that the bed formed on the line merging station was not as smooth as the bed formed by conventional raster.

Further work is needed to optimize the WC-Co slurry for use with the line merging station. The slip casting time of individual slurry lines needs to be increased in order to allow lines to be deposited next to each other while still wet. Also, pressure

pulses due to the peristaltic pump and the turnaround g-forces need to be eliminated or minimized to a point they no longer affect the powder bed.

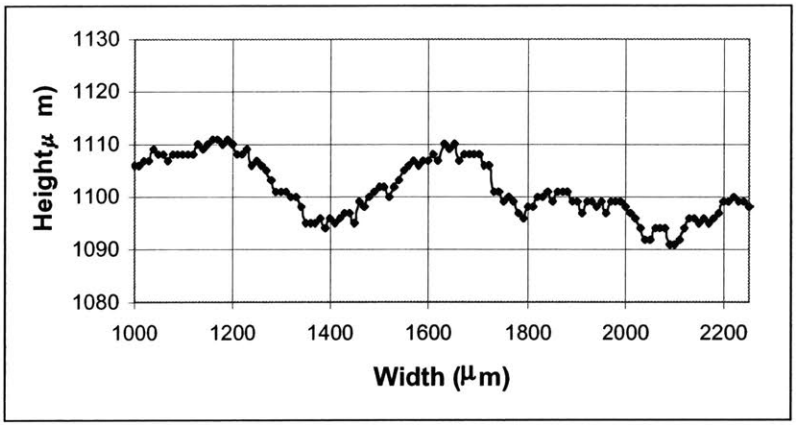

Figure 43: Surface roughness of a WC-Co powder bed formed on the line merging station with 313um slurry line spacing. Standard Deviation is 5.46μm.

4.3 Binder Deposition

This section reports the work performed with multiple binder printing techniques. The methods of binder printing will be explained. The parts formed from the methods are documented and compared, and the results from sintering the parts are reported. The section concludes with a discussion on possible origins of the voids found in the printed parts.

4.3.1 Continuous Jet Binder Printing and Extrusion Geometries

Continuous jet printing encompasses two methods of binder printing. The first, and the simplest, jets of a stream of binder through a small orifice and reaches the powder bed as a uniform column of liquid. The second method uses the same orifice but breaks the stream into uniform droplets using a piezoceramic before it reaches the powder bed.

This first part of this section will focus on the results obtained with the extrusion geometries. These simplified part geometries were used in order to avoid problems

encountered with the charge and deflection method of printing ethanol based binder. The method of Continuos Jet (CJ) printing will be discussed in the latter part of this section.

4.3.1.1 Extrusion Geometries

Charge and deflection of the binder stream is not used when creating extrusion geometries. This limits the shape of the part that can be printed with this method. Figure 44 illustrates the geometries used for testing. The term Extrusion Geometry is derived from the fact that the shape of the parts is a 2-D image that has been stretched, or extruded, in the third dimension. This third dimension lies along the fast axis of the 3DP machine. One advantage of this method, other than avoiding charge and deflection problems, is that the binder stream remains as a solid cylinder of fluid for the working distance used. This forms a printed part where the edge definition the straightness of each binder line primitive is the best case that can be accomplished with the system. Any roughness to the edge of a binder line primitive is due to wetting and spreading issues or part etching during the retrieval process since the binder is deposited as a perfectly straight line.

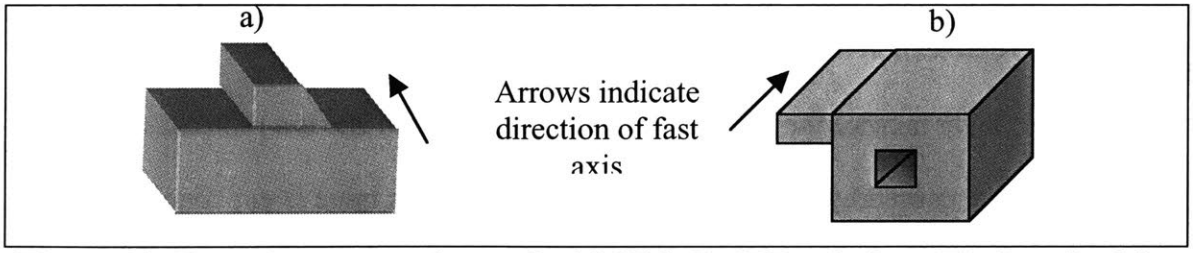

Figure 44: Extrusion geometries used with WC-Co 3DP printing. The length of the jetted bed sets the depth of the part.

A reliable binder stream allowed for the improvement in part resolution depicted in Figure 45a and b. Low binder dose results in delamination between layers and low green strength, as seen in Figure 45a. Figure 45b is the result of optimized binder dose

and layer height to provide good part resolution and strength. Figure 46a shows a representative image of the sidewall of an extrusion geometry printed with PAA binder. Some pitting is seen due to sonication, as well as poor stacking of layers.

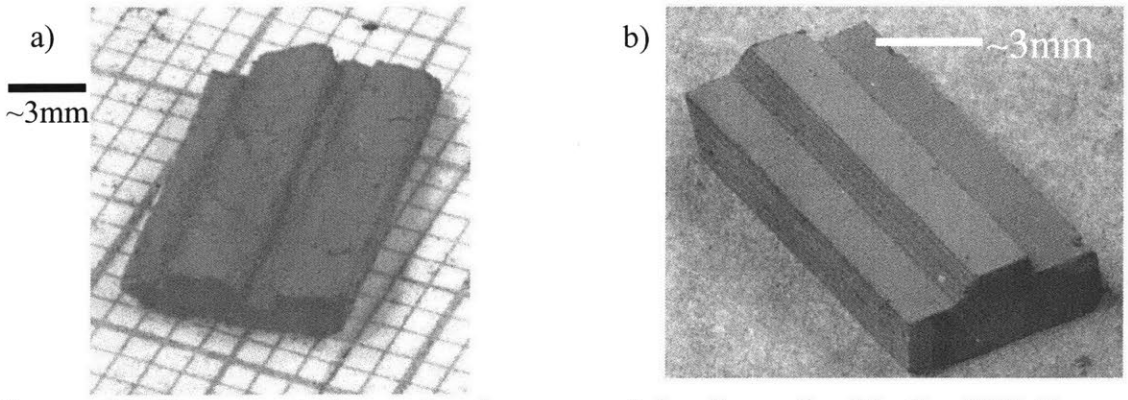

Figure 45 Representative extrusion geometries formed with the WC-Co system printed with PAA-Ethanol binder a) Initial results and b) Final results

Tests with PEI printed extrusion geometries were also performed with powder beds made with the Polyvinylpyrrolidone (PVP) dispersant. These test samples showed improved surface finish of the sidewalls and base of the parts, which are the most susceptible to pitting and etching during sonication. Figure 46 compares the sidewall roughness of a PAA and PEI printed geometry. Both samples were sonicated to remove excess powder, but the extrusion geometry printed with PEI does not show signs of pitting. The delineation of the layers in Figure 46b is not due to etching between layers. Each visible layer is twice the height of the slurry layers used and is a remnant of a binder spreading issue caused by the bed surface roughness. This issue is explained further in the next section.

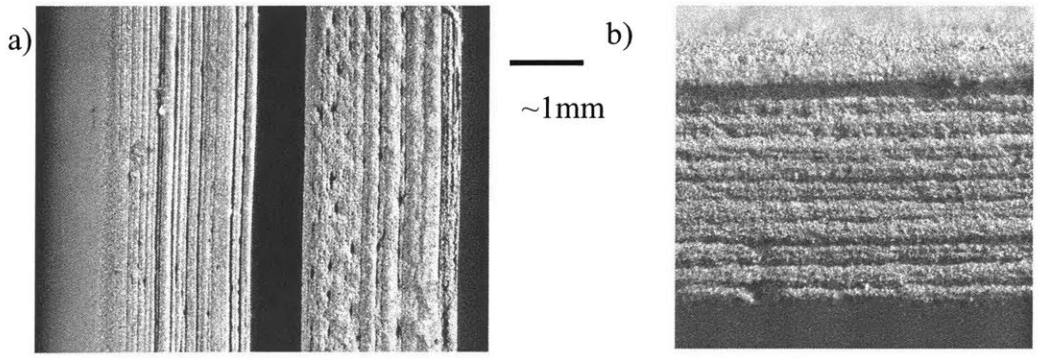

Figure 46 Comparison of sidewalls from PAA printed extrusion geometry a) and PEI printed b) after sonication.

4.3.1.1.1 Sintering of Extrusion Geometries

The sintering of the extrusion geometries formed at MIT, as with the powder beds discussed above, was performed at Kennemetal and Valenite. The same sintering schedules were used, although the binder burnout step was modified due to the additional organic content introduced by the binder. Initial sintering results showed large voids in the powder bed, as well as graphite clusters formed due to excessive carbon content, shown in Figure 47. The voids are approximately 8 μm in diameter and appear as dark circles in the image, while the graphite clusters are made up of much smaller spheres of graphite which group together to form the grayer patches.

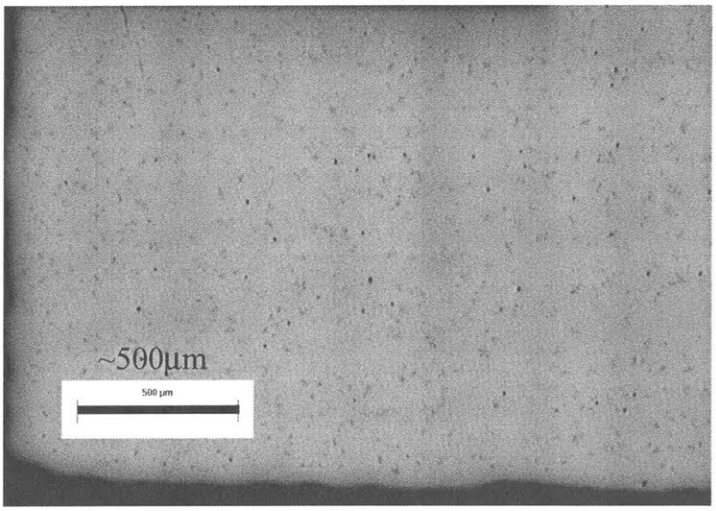

Figure 47: Cross section of sintered WC-Co extrusion geometry. 0.5wt% Solsperse, 5.8Vol% PAA binder.

A second powder bed was printed under the same slurry and binder conditions, as well as a powder bed where the binder was replaced by ethanol, were made in order to determine the origin of the large pores found in the sintered part. The powder bed that was reprinted was sintered without removal of the printed part. Figure 48a shows a cross section of the sintered bed, which had voids arranged along the layers of the printed bed. Of note is the lack of carbon porosity, which was eliminated by adjusting the binder burnout schedule. The area in the sintered cross section with high void content appears to begin about 1mm from the bottom of the bed, which coincides with the first layer that binder printing began. Ethanol was printed into the second powder bed to determine if depositing a liquid onto the powder bed rearranged the already slip cast powder by causing in to redisperse and then re-cast with voids. The results, shown in Figure 48b show no voids in the sintered powder bed.

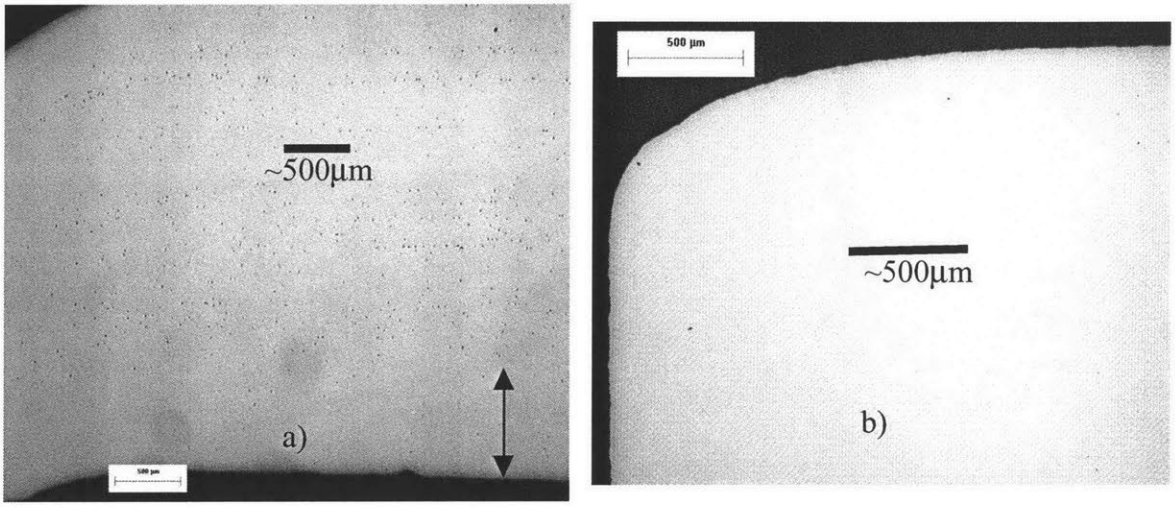

Figure 48 Cross sectional view of a) PAA printed powder bed using same slurry parameters as Figure 41 and b) ethanol printed powder bed. Arrow indicates approximate distance from bottom of bed where binder deposition was begun.

The voids seen in the sintered beds were also present in the green beds. Cross sections of un-sintered samples of the powder bed shown in Figure 48a were viewed under the SEM after potting and polishing. SEM images were taken from areas of the bed with and without binder. The magnification was 150X, which gave a sampling window of 0.414mm^2. The total number of voids in each window was counted and values were reported as number of voids per unit area. The results showed that for areas outside of the binder printed regions there was an average of 37 pores/mm^2 with a standard deviation of 16 over 7 samples. There was an average of 184 pores/mm^2 with a standard deviation of 39 over 6 samples within binder printed areas. The pattern of voids lining up along jetted layers is apparent from inspection of the SEM images taken from within the binder printed region. The spacing between the layers of lined up voids is approximately the same as the layer height of 35µm. Incorporating the $\pm$6µm for surface roughness could explain the fact that the pores do not line up exactly, and are not always 35µm from pores above or below it in the SEM image.

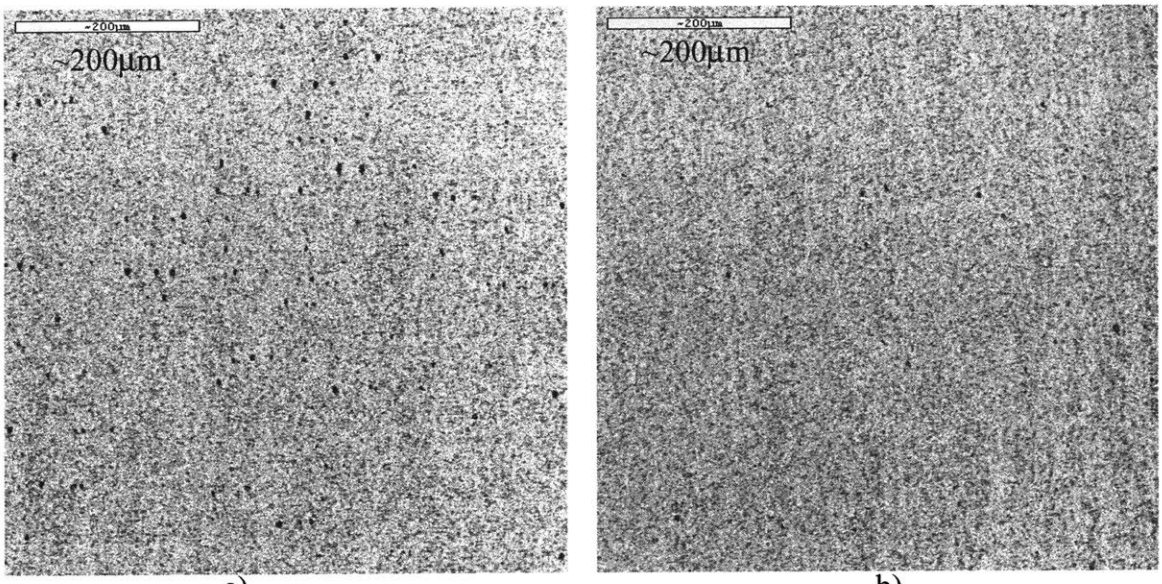

a) b)

Figure 49: SEM image of cross section of green WC-Co powder bed a)inside and b) outside of the binder printed area. LS=200µm, LH=35µm.

The results show that the voids are formed during the deposition of slurry on a powder bed that has been printed with binder. The shape of the voids within the printed region are similar to those outside the printed region. The size of the voids in the printed region average a size of 7.5 µm, while the average size of the voids outside the printed region is 3.5 µm. The frequency of void formation is also much higher in the binder printed areas. This suggests that the mechanism of void formation is already present in depositing slurry, but is caused to occur more frequently by the presence of the PAA binder. More about the possible origin of the voids is discussed in section 4.3.3.

Large voids were present in extrusion geometries printed using the aqueous PEI binder as well as a large amount of carbon porosity. These parts had a pore rating of A04-B00-C5. The sintered parts also showed a low density of 14.0g/cc, 96.8% of theoretical. The binder content of the printed parts was high, approximately 7.2vol% of the powder. Future work may focus on decreasing this content to lessen the chance of carbon porosity being formed during sintering.

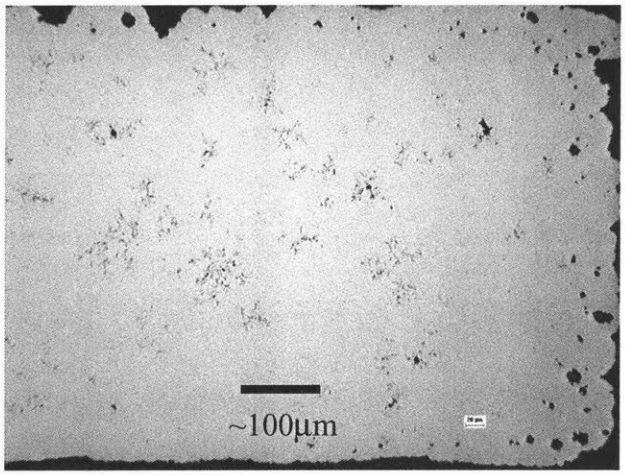

Figure 50: Cross section of sintered WC-Co extrusion geometry using aqueous PEI binder.

4.3.1.2 Continuous Jet Printing

One method of ink jet printing binder material into a powder bed is called Continuous Jet (CJ) printing. With CJ printing a stream of binder is broken into droplets at the Rayleigh frequency using a piezoelectric actuator. The stream can be turned On and Off by activating a Charging Cell which gives the droplets in the stream a net charge. A potential is set up between the plates of the charging cell when the print head is off, causing free charges to be driven from the end of the binder stream that is in the cell. The droplets will then carry net charge within them since the droplet formation occurs within the cell. Uncharged droplets pass straight through a Deflection Cell, while charged droplets are deflected into a Catcher. This allows for control over where binder is printed as the print head is raster scanned across the powder bed. Figure 51 illustrates this On and Off control. Initial experimentation on WC-Co using this method caused delays in testing due to problems encountered with the ethanol binder. The low surface tension of the ethanol caused the binder to easily wet all the print head surfaces making flooding a common problem. Charging the droplets was also difficult due to the low

dielectric constant of the ethanol, which led to difficulties in deflecting the stream into catch and allowed no control of where the binder was printed. It could not be determined if the defects in the printed parts originated from a materials incompatibility issue or an issue with binder stream stability with these problems. The method described in the previous section was devised in which dropletization, charging, and deflection was not needed, in order to overcome this problem.

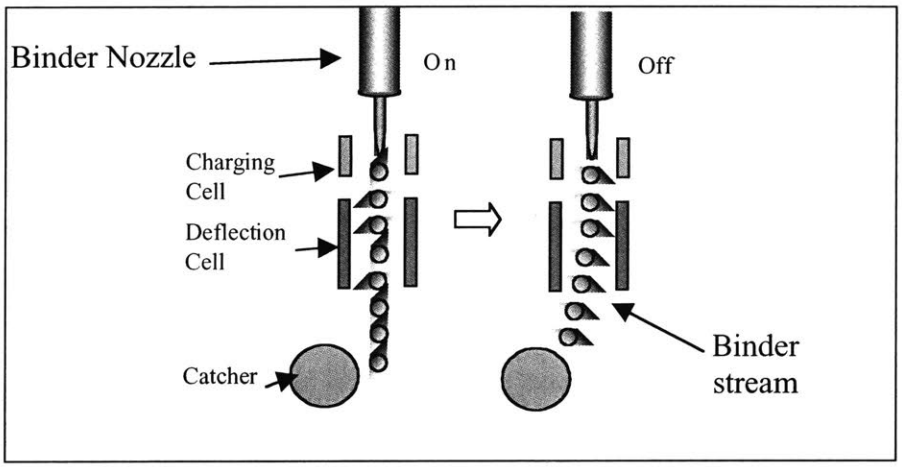

Figure 51: Major components of a Continuous Jet print head and its operation.

The problems described above were encountered in the test 3DP machine. Another 3DP machine, named the Alpha Machine, had a superior print head that did not suffer from constant flooding and poor control of the binder stream. This machine was available to test the results of CJ printing once the trials with the extrusion geometries were completed. Cutting tool insert geometries were printed on the Alpha machine with the Solsperse slurry, and are shown in Figure 52.

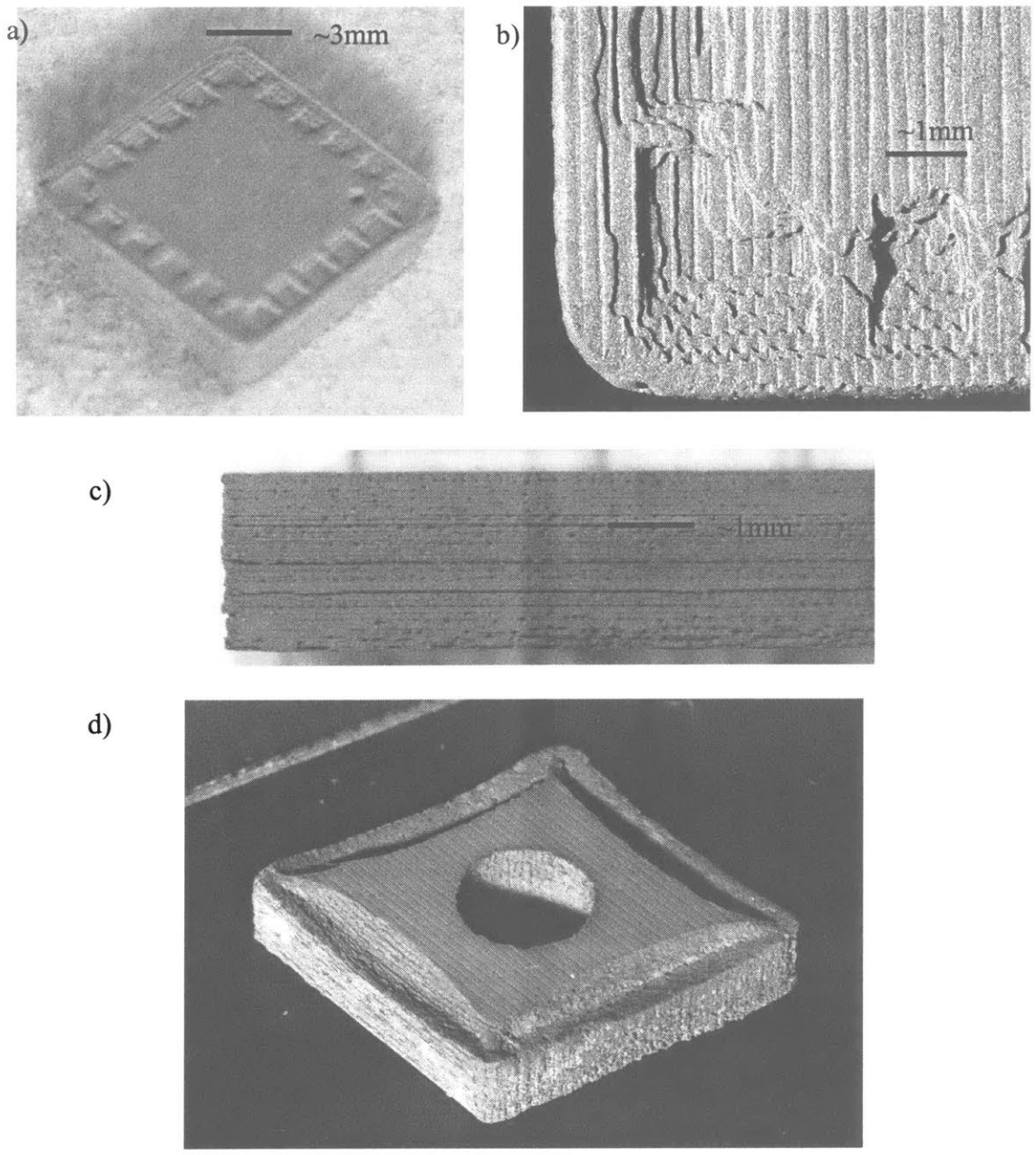

Figure 52: First cutting tool insert printed on Alpha machine using CJ printing of PAA binder a), top view of corner b), sidewall view of a bar geometry printed with the insert geometries c) and second insert geometry printed on the Alpha machine d).

The close up image in Figure 52b illustrates the effect that the surface roughness of a powder bed has on the binder line primitives. The slurry lines of a printed bed are clearly seen running from top to bottom upon examination of the image. Comparison of

the edges of the part that align with and across the slurry lines shows that those that align with the slurry lines are much smoother. The saw-toothed pattern formed on the part edges that cross the slurry lines is staggered from one layer to the next and upon examination of machine parameters it was determined that it was the slurry raster that was staggered, not the binder raster. This suggests that the binder wets further along the "valleys" in the surface of a powder bed to form the saw-toothed edge. Another factor affecting part resolution was the lack of redispersion of the powder bed after curing. Extensive sonication was required during part retrieval to remove the excess powder that caused pitting and some delamination of fine edge features. The effect on sidewall roughness can be seen in Figure 46c, which shows pitting of the side of a bar geometry printed at the same time as the insert shown in Figure 46a and b.

4.3.1.2.1 Sintering of CJ Printed Parts and MOR Bend Bar Results

The sintering of the CJ printed parts showed similar microstructure to the sintered extrusion geometry parts. Large 8μm voids arranged along the layers of the part were seen. The porosity rating for the parts was A06-B02-C06.

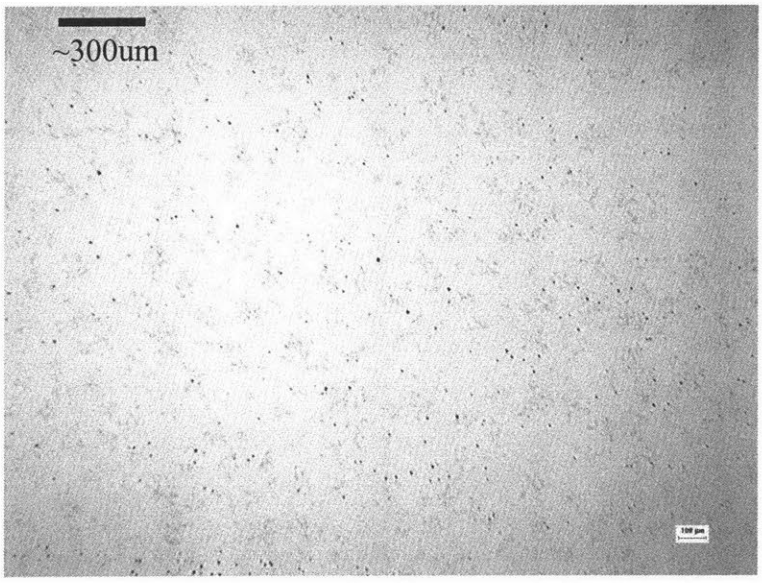

Figure 53 Sintered cross section of insert printed on Alpha machine using PAA binder.

The strength of the bend bars printed using CJ printing were tested with a 4 point bend test. The average values for 6 bars was 253 ksi, which was 65% of the values attained for conventionally pressed bend bars. The poor results were attributed to the carbon porosity.

4.3.2 Drop on Demand Vector Printing

Drop on Demand (DoD) Vector Printing incorporates two new technologies that will be discussed at this time.

DoD printing differs from CJ printing by the fact that for DoD each droplet is formed by one expansion and contraction cycle of a cylindrical piezoelectric that is placed around the binder tubing. This is not the case with CJ printing. Instead, the piezo is tuned to a frequency that will cause the binder stream to naturally form droplets. The droplet formation frequency is approximately 30 kHz for CJ printing, while for DoD printing it is around 1 kHz.

The high frequency of drop formation in CJ printing requires a print speed in the range of 150cm./sec in order to deposit the correct binder dose. The low frequency of operation of a DoD nozzle allows for the second difference between the CJ and DoD printing techniques, which is Vector Printing. The outline of a part can be traced with binder then followed with a raster fill with vector printing. This technique results in better part definition, as is illustrated in Figure 54.

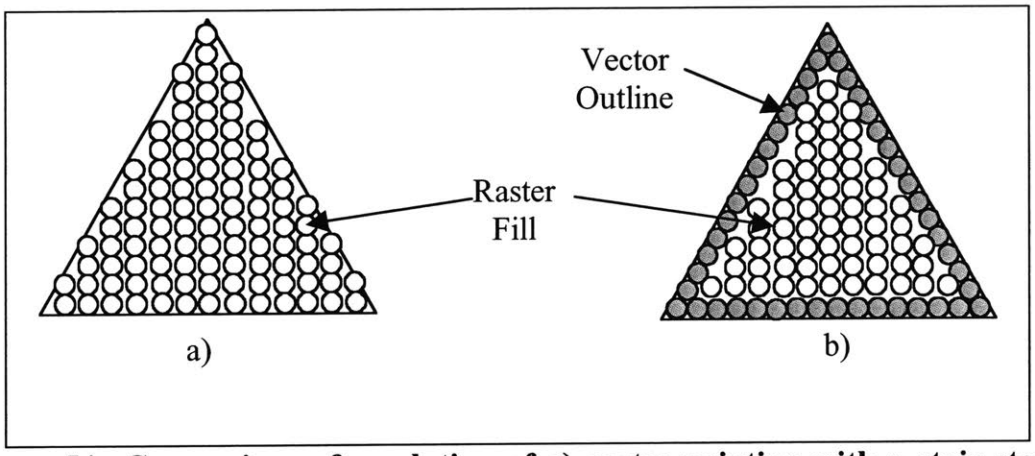

Figure 54 Comparison of resolution of a) raster printing with a stair stepping effect and b) vector printing

DoD printing operates at a low enough frequency to allow print speeds to be in the range of 6.5cm/sec. This is critical in vector printing because at higher speeds the acceleration produced at corners can become extremely high and beyond machine capabilities.

WC-Co insert geometries were printed using this method and the aqueous PEI binder. The simple shape printed was designed to model important features found on cutting tool inserts. Areas of interest were slope of the chip breaker, the sidewall, and the corners. These parts are shown in Figure 55. The visual quality of the Vector DoD parts was much better than those printed using the CJ raster style printing. The roughness of the sidewall in Figure 55c was not seen to change with continued sonication. This

suggests that the roughness was due to a binder spreading issue during printing. This spreading issue is also seen in the rounding of the outside corners of the part, but not the inside corners. Figure 55b is representative of how the inside corner of a part is sharper than the outside.

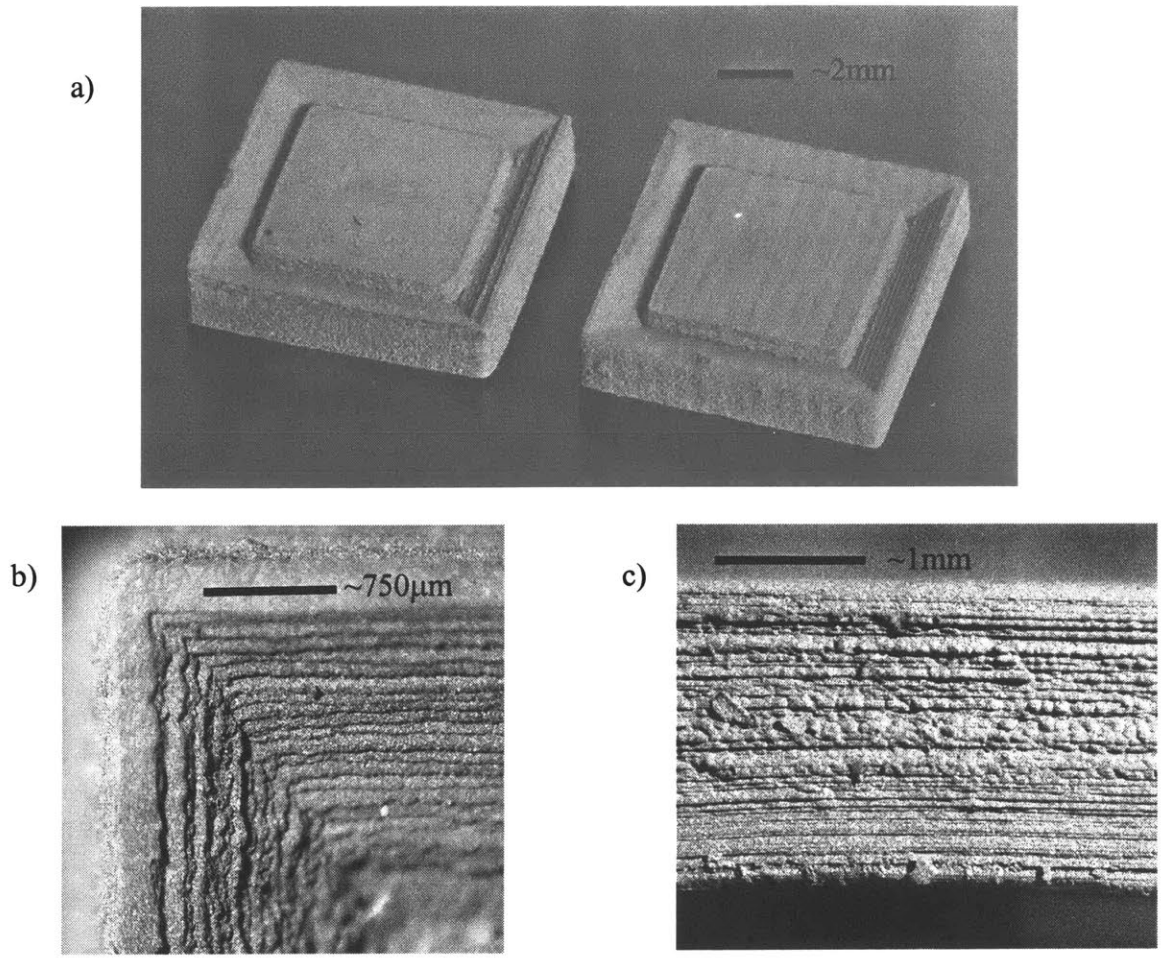

Figure 55: DoD Vector printed geometries for WC-Co powder beds using PVP dispersant and aqueous PEI binder, a)isometric b) close up view of top left corner c) close up view of side wall.

4.3.2.1 Sintered Vector DoD Printed Parts

The WC-Co parts printed using Vector DoD printing used an aqueous PEI binder. Although the parts showed superior surface finish than the CJ printed PAA parts, the

sintering results showed that large blisters between layers and pores were formed, as shown in Figure 56. The amount of A and B porosity was higher than with the extrusion geometries printed with PEI. This is attributed to the higher surface roughness of the DoD powder beds formed on the line merging station. The blisters are believed to be formed during the binder curing step, since the large bulge seen in the top part of Figure 56 was observed before sintering. Further discussion on the possible origin of these blisters is discussed in the next section.

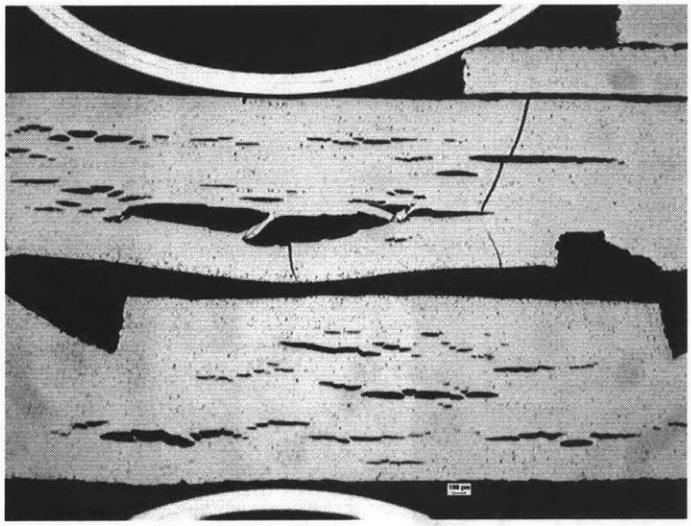

Figure 56: Cross section of two DoD printed WC-Co parts sintered at Valenite

4.3.3 Possible Origin of Voids in Powder Beds

The voids seen in the powder beds discussed in sections 4.3.1.1.1 and 4.3.2.1 are believed to be caused by two different mechanisms. The voids discussed in 4.3.1.1.1 were said to be due to the presence of the PAA binder in the powder bed affecting the deposition of the subsequent slurry layers. Two ways for this to happen are discussed here and are called the "Spreading" and the "Splashing" effects. It is proposed that the

presence of the binder affects the wetting angle of the deposited slurry line for the spreading effect. Figure 57 is an image of the alumina slurry lines being deposited and shows that the outer edge of the slurry line in the already cast samples is not as straight and smooth as the edge that is still wet. This may be a sign that it does move after it has been deposited, and the slurry is wetting out onto the bed a little. It is possible, in this case, that if the PAA increases the wetting contact angle of the slurry edge the chance that the instability depicted in Figure 57b will increase. This increased chance may also explain why the same voids are present in beds without PAA, but at a smaller size and lower frequency.

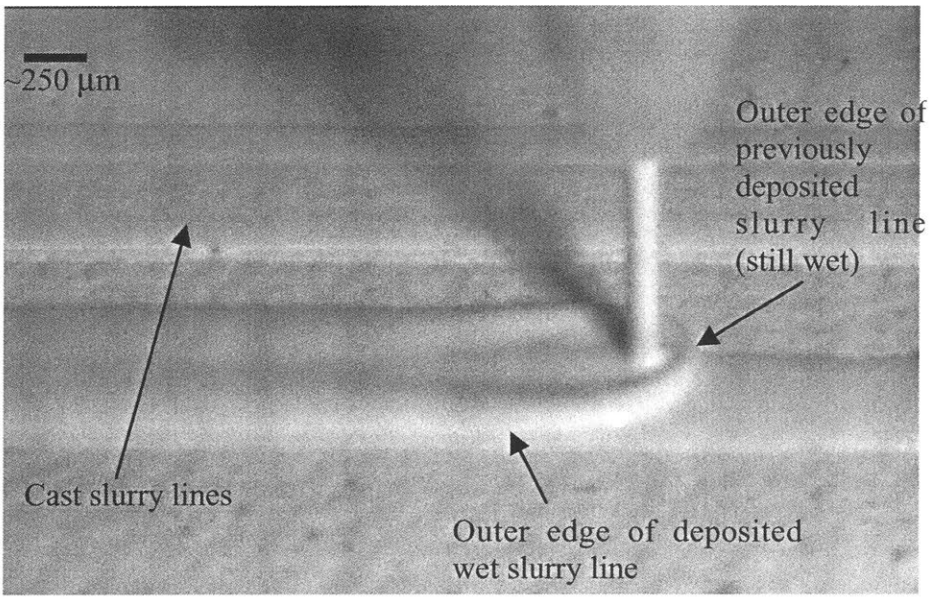

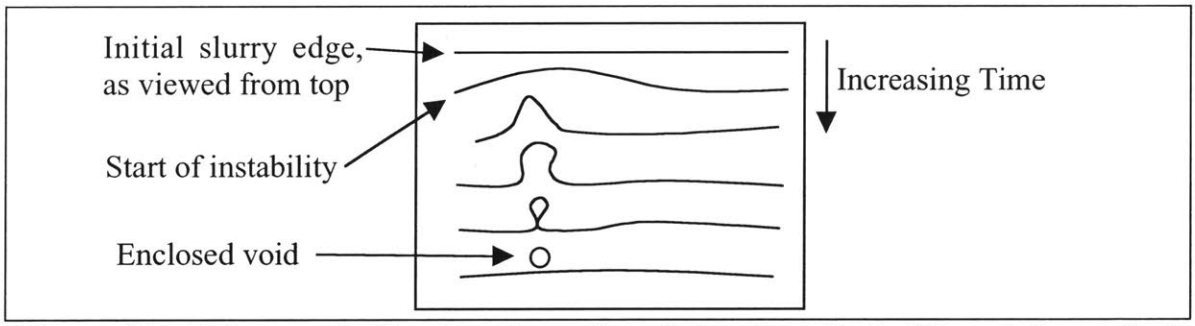

Figure 57: A) Image of Alumina slurry lines being deposited with an inter arrival time of 30 msec[21]. B) Proposed model of void formation due to slurry edge instability (not to scale).

Another possible cause of the voids is that they are formed when the slurry is deposited over top of the edge of a previously deposited slurry line, as shown in Figure 57a. This is the Splashing effect. It is evident from the image that the slurry is quickly pushed across the surface of the powder bed due to kinetic energy. Air bubbles may be entrapped when this happens over the edge of a previous slurry line. The presence of the PAA may make air bubbles more likely to stick to the surface of the bed. Figure 58 shows an image of the cross section of a WC-Co powder bed. The pattern with which the slurry lines stack themselves can be seen at the top of the image. The figure shows that

the size of the voids in the green powder bed is similar to the height of the ridges at the top of the bed. This may be evidence that supports the splashing effect.

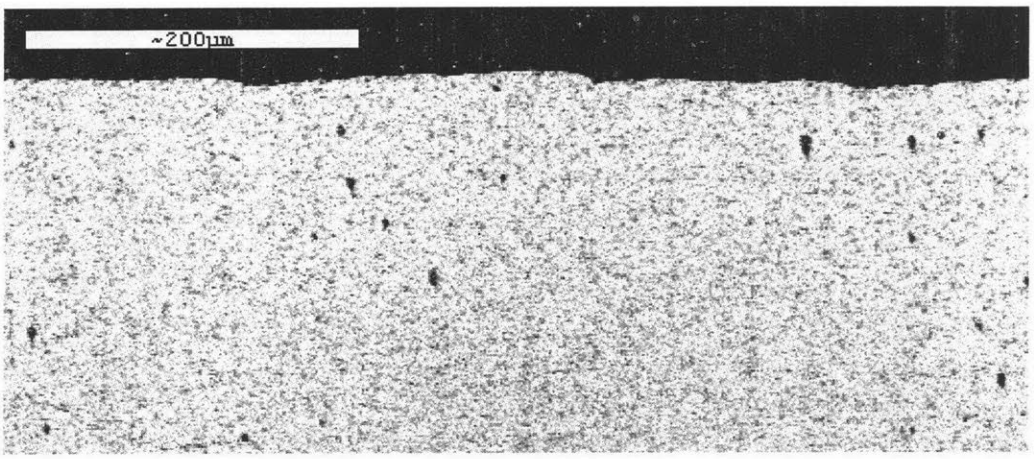

Figure 58: SEM image of the cross section of the top of a WC-Co powder bed (view into fast axis) with *LS* = 200 µm and *LH* = 35 µm.

The parts printed on the TDK machine using the PEI binder showed large blisters, as discussed in section 4.3.2.1. One possible mechanism for their formation is that during binder printing a high bed temperature due to excessive drying causes the binder to segregate to the surface. There is less pore space in the regions with segregated binder. This decreases the permeability of gases evolved during the high heating rate of the binder cure step. The voids then form due to a pressure buildup. The extrusion geometries printed with the PEI at a higher binder content did not form the blisters. The drying temperature was lower during the printing of the extrusions and the method of drying, a heat lamp, was less intense than the forced hot air used with the vector printed parts. This suggests that using a lower drying temperature may help eliminate the cause of the blisters.

4.4 Redispersion

Redispersion is an important element of the part retrieval process as discussed in a previous chapter. It is the result of the osmotic pressure developed in the powder bed when the redispersion agent dissolves into the redispersion solvent. This osmotic pressure causes the unprinted regions of the powder bed to swell and fall apart. Tests were performed on the two WC-Co slurry systems. The first system used the Solsperse dispersant and the second used the PVP dispersant.

4.4.1 Affect of Redispersion in Water on Sintering

A WC-Co extrusion geometry using Solsperse slurry was created for testing the affect that redispersion in water had on the sintered microstructure. The extrusion geometry was divided into parts before immersion. 2 pieces were redispersed in water and 1 was redispersed in methanol. The amount of time that the parts were in contact with water varied from 30 minutes to 1 hour. The parts were placed in methanol after they were retrieved from the water. The liquid was wicked out by placing the part on a paper towel. The procedure was repeated in order to remove as much water from the part before it was left to dry in air. The 3 samples were sent to Valenite for sintering and microstructural analysis. The results showed no discernable difference between the parts redispersed in water or in methanol. This supported the results discussed in Chapter 2, in which the increase in total oxygen content measured for WC and Co powders exposed to water was deemed acceptable.

4.4.2 Redispersion of Polyvinylpyrrolidone Powder Beds

Powder beds were formed using a 24vol% WC-Co slurry with 0.5wt% PVP 10,000 dispersant and PEG concentrations of 0.5 and 0.6wt% using the S-3DP method. Redispersion was tested using water and methanol as a redispersion solvent. Redispersion of the powder beds was seen when they were placed in water either before or after a binder cure step. No redispersion was seen when they were placed in methanol.

4.4.3 Redispersion of Solsperse Powder Beds

Powder beds formed by the S-3DP process and using the Solsperse dispersant were tested with Poly(ethylene glycol) (PEG) and Poly(propylene glycol) as redispersing agents. Both PEG and PPG had a molecular weight of 400. Either water or methanol was used as the redispersion solvent. PEG and PPG were used in varying amounts from 0.5wt% to 1.6 wt% of the powder.

The results of the testing were the same for all of the Solsperse systems. The powder beds showed some signs of redispersion directly after formation. However, after a heat treatment of 150°C for 1hr in an argon atmosphere to simulate the binder curing step the powder beds did not redisperse in water or methanol. The bed did not redisperse after aging in air for 2 hours. If a powder bed was placed in a dessicator right after formation, the length of time before it did not redisperse was extended to approximately 24 hours.

The weight gain of the powder beds was measured to be 0.26 wt% after aging in air for one day. This value was close to the predicted gain of 0.23wt% calculated by assuming all of the weight gain was due to the PEG and Solsperse in the bed absorbing moisture from the air. Weight gain values of 20% and 3.5% for the PEG and Solsperse,

respectively, in air were previously measured and used in the calculation. In order to determine if the affect of aging in air was reversible and was caused by absorbed moister, aged powder beds that no longer redispersed were dried in a vacuum oven to remove absorbed moisture. The powder beds did not redisperse after drying.

The lack of redispersion in the Solsperse system is thought to be due to a chemical reaction taking place with the Solsperse. It is believed that the Solsperse polymerizes at the amine end groups with the PEG. Upon comparison with the PEI binder which was observed to crosslink and form an insoluble compound, the Solsperse has the same functional group with which to react. Furthermore, the Glycerol added to PEI and PAA as a crosslinking agent contains the same functional group, a hydroxyl, as the PEG. The Solsperse has shown a tendency to react when mixed with other polymers. It was observed to react with the Poly(vinyl acetate) (see section 3.2.3). It was discovered that when the Solsperse and the PEG were mixed together in a 1:1 wt% ratio, that the two polymers have a miscibility gap. The mixed polymers separated into two phases, but both polymers were present in both. One phase appeared to be Solsperse rich, while the other was PEG rich.

5 Conclusions and Future Work

The examination of the WC-Co system in order to produce cutting tool inserts through Slurry Based 3-Dimensional Printing (S-3DP) showed that a materials system comprised of a Polyvinylpyrrolidone dispersant, Poly(ethylene glycol) 400 redispersant, Isopropyl Alcohol slurry medium, and an aqueous Polyethylenimine binder is capable of creating the desired cutting tool insert geometries with good part resolution using Vector Drop on Demand binder printing. The system was also capable of achieving sufficient powder bed redispersion for part retrieval. Further work is needed, however, to overcome deficiencies in the sintered product. The voids and blisters seen in the sintered inserts will need to be eliminated before a determination can be made as to whether the green density achieved is sufficient for sintering to full density.

Another WC-Co materials system using the Solsperse 20,000 dispersant formed fully dense sintered powder beds with a good porosity rating of A01-B00-C00. The system was unsuitable for S-3DP however, due to lack of redispersion of powder beds after undergoing a binder cure step or aging in air for short times.

The jetting characteristics of the WC-Co slurry system was observed to be sensitive to air leaks within the system. Attempts at on-off slurry control, achievable with aqueous slurries, failed with the alcohol slurry. Both the sensitivity to air leaks and the lack of success of on-off slurry control were attributed to the volatility of the alcohol slurry and the quick formation of agglomerates during drying. The system was also observed to be sensitive to settling in the slurry, and special attention was needed to ensure low residence times and smooth transitions for all slurry lines in the handling system. Despite the apparent sensitivity to drying effects, it is recommended that future

work on a method for conserving slurry during printing be developed. A current proposed design involves a catcher for the slurry that collects slurry when it is not jetting a bed. The slurry in the catcher is in a similar loop to that used with the pressure vessel slurry handling system. Before returning to the main reservoir, the slurry is passed through a filter to collect any agglomerates which have formed.

Future work for the WC-Co system will focus on optimizing the formation of powder bed layers using the layer forming station. Focus should be place on eliminating blisters and voids in the sintered cutting tool inserts. This involves an examination of the effects of printing parameters as well as modification of the slurry composition to decrease the casting rate of individual slurry lines.

REFERENCES

[1] Zanetti, Giovanni, and Bice Fubini. J. Mater. Chem. **7**(8) (1997) 1647-1654.

[2] Gothelid, M., S. Haglund, and J. Agren. Acta Metallurgica, **48** (2000) 4357-4362.

[3] Holman, Richard. Journal of Colloid and Interface Science. **247** (2002) 266-274.

[4] Ulhand, Scott. Journal of the American Ceramic Society. **84** [12] (2001) 2809-2818.

[5] Ulhand, Scott. Fabrication of Advanced Ceramic Components using Slurry-Based Three Dimensional Printing. **Ph.D.**, *Department of Materials Science and Engineering, Massachusetts Institute of Technology*, 2000.

[6] Hiemenz, Paul, Raj Rajagopalan. Principles of Colloid and Surface Chemistry. 3rd Ed. Marcel Dekker: NY, 1997.

[7] Brandrup, J., et al. Polymer Handbook. 4th Ed. John Wiley and Sons, NY: 1999.

[8] Huang, L., and K. Nishinari. Journal of Polymer Science, Part B: Polymer Physics. **39** (2001) 496-506.

[9] Conway, B. E., and M. L. Lakhanpal. Journal of Polymer Science. **46** (1960) 93-111.

[10] Kagemoto, Akihiro, et al. Die Makromolekulare Chemie. **150** (1971) 255-261.

[11] Eliassi, A., and H. Modarress. European Polymer Journal. **37** (2001) 1487-1492.

[12] Holman, Richard. Effects of the Polymeric Binder System in Slurry-Based Three Dimensional Printing of Ceramics. **Ph.D.**, *Department of Materials Science and Engineering, Massachusetts Institute of Technology*, 2001.

[13] Guo, David. Unpublished work.

[14] Morrisette, Sherry. Personal communication.

[15] Andersson, Karin, and Lennart Bergstrom. Refractory Metals and Hard Materials. **18** (2000) pp121-129.

[16] Russ Yeckley, PhD. Kennemetal. Personal Communication.

[17] Anna Finlayson, Unpublished work.

[18] Micromeretics, AutoPore 2 9220 Operator s Manual V3.03. 1993

[19] Heimenz, Paul, and Raj Rajagopalan. Principles of Colloid and Surface Chemistry. 3rd Ed. Marcell Dekker, NY: 1997.

[20] Skeist, Irving, Handbook of Adhesives. 3rd Ed. Van Nostrand Reinhold, NY: 1990, pp 466-467

[21] Ben Polito, Unpublished Work.

[22] Guo, David. Unpublished Work.